



Efficient multiscale methodology for local stress analysis of metallic railway bridges based on modal superposition principles

Cláudio S. Horas^{a,*}, Abílio M.P. De Jesus^b, Diogo Ribeiro^c, Rui Calçada^a

^a CONSTRUCT-LESE, University of Porto, Faculty of Engineering, Porto, Portugal

^b INEGI, University of Porto, Faculty of Engineering, Porto, Portugal

^c CONSTRUCT-LESE, School of Engineering, Polytechnic of Porto, Porto, Portugal

ARTICLE INFO

Keywords:

Railway bridges
Riveted joints
Fatigue
Submodelling relation
Modal superposition
Experimental validation

ABSTRACT

This paper presents an advanced submodelling methodology for local stress analysis of complex details of existing metallic railway bridges. The fatigue assessment of connections of large structures based on local methods leads inherently to a multiscale problem that can only be solved by adopting efficient numerical procedures. Aiming to overcome such limitations that influence the analysis process, submodelling techniques and modal superposition principles are combined to fully represent numerically the local geometrical, material and contact properties of the fatigue-critical details. The results of experimental *in situ* tests are proposed to characterise the numerical models and respective multiscale relation, implementing optimisation and validation procedures. In this work, the suggested efficient multiscale methodology for stress analysis aims to allow the subsequent local fatigue assessment, according to the real mechanism of loading transference, reducing sources of conservatism. All numerical procedures and respective validation thru experimental techniques are illustrated using a real case study.

1. Introduction

In the past two decades, several European countries have made considerable efforts to improve the existing railway infrastructures and plan new lines on which trains can operate safely at higher speeds. In 2019, the European Commission defined the European Green Deal with the aim of achieving climate neutrality by 2050, establishing that a substantial part of the 75% of inland freight transported currently by road should shift onto rail and inland waterways [1].

The planned railway network demands the existence of a considerable number of infrastructures, such as bridges and tunnels. Naturally, as axle loads and circulation speed increase, the requirements for a safe operation on railway lines are more restrict, leading to the necessity of building new structures or verify the integrity of the existing ones. The generated complex dynamic loadings are responsible for structural problems that must be considered. Among the mentioned structural issues, progressive damage due to fatigue phenomenon should be highlighted as a major concern, as it may lead to severe cracks in metallic elements. In this context, the development of advanced tools for structural analysis has been assumed as critical, in order to properly evaluate the safety requirements for the current and future service conditions, in line with the real response of structures.

Different procedures may be used to assess fatigue damage, namely global and local stress-life methods, notch strain methods and Fracture Mechanics based methods [2–6]. For a certain structural detail, global S-N methods have been proposed to establish a relation

* Corresponding author at: University of Porto, Faculty of Engineering, Rua Dr. Roberto Frias, 4200-465 Porto, Portugal.
E-mail address: claudiohoras@fe.up.pt (C.S. Horas).

Nomenclature

$BDCOs$	boundary conditions
$BDCOs_j$	boundary conditions of the j^{th} vibration mode
$BDCOs_{sw}$	part of $BDCOs$ due to the permanent loading
C_{-}	damping matrix
E	Young's modulus
F	nodal forces vector
f_j	nodal force of the j^{th} vibration mode
f_{yd}	yielding stress
K_{-}	stiffness matrix
k'	cyclic strain hardening coefficient
M_{-}	mass matrix
\overline{MAC}	average modal assurance criterion
N_f	necessary number of cycles to the crack initiation (range l)
n_i	number of cycles related to $\Delta\sigma_i$ and N_i (range l)
n'	cyclic strain hardening exponent
u	column matrix of displacements
\dot{u}	column matrix of velocities
\ddot{u}	column matrix of accelerations
w_j	modal frequency of the j^{th} vibration mode
Y_j	modal coordinates of the j^{th} vibration mode
α_y	thermal expansion coefficient (yy-direction)
$\overline{\Delta e_f}$	average frequency error
ξ_j	modal damping coefficient of the j^{th} vibration mode
ρ	density
ν	Poisson ratio
σ	stress quantity
σ_j	modal stress quantity of the j^{th} vibration mode
σ_{sw}	part of σ due to the permanent loading
φ'	amplification factor for the dynamic loading
φ''	amplification factor for the irregularities of the track and vehicles imperfections
ψ	generic damage parameter
ψ_j	modal damage parameter of the j^{th} vibration mode
ψ_{sw}	part of ψ due to the permanent loading

between the applied nominal stress range and the fatigue resistance, with this approach as the most common in the applicable standards and guidelines, including Eurocode 3, Part 1–9 [7]. Nonetheless, relevant drawbacks may be highlighted, taking into account that a limited number of S-N curves are available and may not properly reflect the local structural behaviour of geometries different from those in the origin of such relations. Also, different constructional steel grades are not distinguished, which may be a drawback mainly when assessing older materials. Thus, alternative local fatigue approaches may be seen as more accurate than the global S-N approaches. In fact, the applicability of those calculation strategies based on local quantities has been gaining importance to evaluate fatigue damage, with the aim of performing the fatigue assessment of details not covered by the available catalogues of S-N curves, distinguishing the damage evolution related to the initiation and propagation of cracks [8–12].

However, the accurate calculation of local mechanical quantities can hardly be performed due to the numerical difficulties underlying the multiscale problem. Frequently, the size of Civil Engineering structures is of the order of metres or kilometres and the fatigue damage areas are of the order of millimetres or below, which clearly raises a multiscale problem characterised by the complexity of the required numerical models, calculation processes and consideration of the applied dynamic load histories. Due to such challenges, high computational costs are expected, in particular as a result of the geometrical refinement at hot-spots for the crack initiation or in existing cracked areas, even when this modelling detail is not expanded to remote locations. In the past few years, important progress in modelling techniques has been made based on the development of computational capabilities. Submodelling approaches integrated into calculation procedures have been implemented, accounting for the interaction between global and local data, allowing to consider global modelling simplifications without neglecting the accurate assessment of local stress and strain fields [9,13–16]. Combining the implementation of submodelling techniques with modal superposition concepts, efficient fatigue evaluations may be performed. For the crack initiation assessment, local methods, such as the relations suggested by Basquin [17] or Morrow [18,19], may be considered, accounting for eventual material nonlinearities by implementing elastoplastic post-processing according to the analytical models proposed by Neuber [20] or Glinka [21–23]. After, in order to evaluate the propagation of a given crack,

Fracture Mechanics based approaches may be adopted.

Concerning the methods to solve the dynamic problem, the direct time-integration has been chosen as a reference approach to assess fatigue damage in small structures, using algorithms such as the Newmark [24] or the Hilber-Hughes-Taylor (HHT) [25]. However, regarding dynamic calculations in large bridges, these algorithms usually require the analysis of a single numerical model during thousands of load steps mutually dependent. As mentioned above, a global model of a large bridge cannot reflect the local geometrical detail, which leads to an unreliable numerical representation of the response of certain connections and respective inaccurate damage assessment based on local fatigue approaches. Also, even if the numerical modelling is simplified, for large bridges, solving the dynamic problem using direct time-integration algorithms may be impossible due to computational demands or may lead to computational times not compatible with the pace of design or monitoring operations. In order to overcome these issues, the modal superposition of local parameters, such as stresses, strains and stress intensity factors may be adopted. As demonstrated by Horas et al. [26,27], localised material or contact nonlinearities do not affect the global structural behaviour that remains linear and therefore possible to be analysed superimposing a limited number of vibration modes.

Considering this background, combining local fatigue methods with the implementation of submodelling techniques and modal superposition concepts, the local response at a certain hot-spot may be assessed accurately and efficiently. Horas et al. [26,27] proposed different approaches to evaluate fatigue issues based on local parameters, with the respective validation being performed using reference solutions (theoretical validation), considering simple case studies (i.e., simple supported beams). Nonetheless, the respective implementation to real complex structures requires further advances in organisation, calibration and validation procedures to increase the reliability of the fatigue assessment. Thus, this paper demonstrates the application of a multiscale methodology for local stress analysis of metallic railway bridges, aiming at future fatigue assessment based on local methods (not covered in this work), investigating complex geometries such as riveted ones and allowing the infrastructures manager to perform efficient and generalised safety checks. The steps of the proposed methodology, including their experimental validation, are discussed in this research.

2. Theoretical background

In this section, the critical aspects underlying the idealised efficient multiscale methodology are described, including the required theoretical concepts, namely: (i) modal superposition principles; and (ii) submodelling techniques involving modal quantities. A general workflow is proposed to define the interaction between the different scales of analysis, assuming three levels of assessment, from the global scale to that associated with local fatigue damage (see Fig. 1).

In Fig. 1, the critical modelling tasks required to compute local results necessary for the assessment of the initiation and propagation of cracks are sequentially described, from the global scale to the fatigue damage one (from i) to iii)). Firstly, i), the structural system must be analysed from the global point of view (e.g., using FE beam elements), which is a classical and reference approach in the design of new structures or in the verification of the integrity of existing ones. Currently, the calculations performed at this scale dominate the fatigue assessment performed by civil engineers, adopting S-N curves to transform nominal stress measures into local quantities by incorporating the local stress raisers in the definition of those S-N relations. Nonetheless, the available fatigue strength

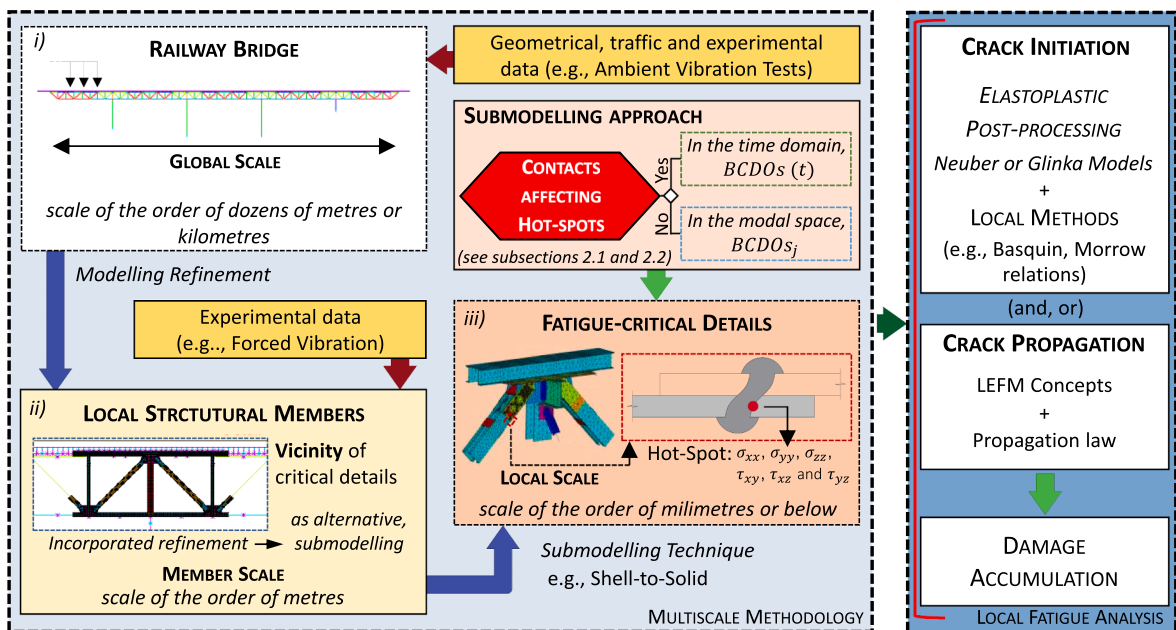


Fig. 1. Efficient multiscale methodology based on submodelling relations aiming at local stress analysis and subsequent fatigue assessment of existing metallic railway bridges.

curves based on nominal stresses may be hardly applicable to a large variety of details of existing bridges without assuming relevant conservative approximations, due to geometrical and material differences. Therefore, the implementation of the linear damage accumulation method suggested in EN1993-1-9 [7] should only allow defining the fatigue-critical details of a certain structure, following a philosophy of multiscale analysis from the global to the local one. Afterwards, in ii), an intermediate modelling at the scale of the local structural members related to the connections of interest should be conceived using shell elements. Depending on the computational demands, a refinement may be incorporated into the global model (beam-to-shell link) or an independent submodel may be built, in this case relating the latter to the global one through a submodelling technique (e.g., beam-to-shell coupling). Finally, the boundary conditions (BDCOs) obtained at the member scale should be imposed on the volumetric submodel of a given critical connection (solid FE elements), which must allow representing numerically all the local geometrical, material and contact characteristics (e.g., beam-to-solid coupling), iii). At this level of modelling, the local stress analysis may be performed to implement local fatigue methods, with this multiscale methodology being theoretically generalisable to a broad variety of connections. Experimental data obtained from Ambient Vibration Tests (AVT) or forced vibration tests should be considered to optimise and validate the conceived models and the established submodelling relations, increasing the accuracy of the numerical results. The reliability of the suggested modelling strategies depends on those experimental validations performed at the different scales, whose relevance is demonstrated and discussed in this paper.

In the following subsections, the theoretical principles underlying the calculation strategy involving local modelling techniques are presented, with these latter being leveraged by modal superposition concepts, which allows solving the dynamic problem in affordable computational times.

2.1 Modal superposition principles

Variable railway loadings may lead to fatigue issues that depend on the structural properties of the loaded structural system. The geometrical and material characteristics of the bridge allows defining values such as mass, stiffness and damping that influence the structural response on the resistance side. Also, for a certain loading at a given speed, the applied forces influence the dynamic behaviour on the loading side. Consequently, the dynamic response of a structural system with N degrees of freedom (DOFs) may be evaluated solving the following system of equations for each time instant t :

$$M \ddot{u}(t) + C \dot{u}(t) + K u(t) = F(t) \quad (1)$$

in which, related to the N degrees of freedom, M , C and K are, respectively, the matrices of mass, damping and stiffness, each composed of $N \times N$ terms. Concerning the loading, $F(t)$ is the column matrix of nodal forces with $N \times 1$ values. Regarding the response, $u(t)$, $\dot{u}(t)$ and $\ddot{u}(t)$ are, respectively, the column matrices of displacement, velocity and acceleration that represent the dynamic response of the structural system, also defined by $N \times 1$ terms. In a classical calculation strategy based on direct time-integration algorithms, the presented system of equations is solved for each time step, with each time instant t being dependent on the previous $t-1$, leading to an indivisible structural analysis that has to be carried out using a single calculation process. For large bridges, such computational demands should require unsustainable computation times, as a considerable number of degrees of freedom N is necessary to define the global response and the local ones of interest, for the variety of traffic loadings to be considered (very large number of load steps). Nonetheless, when the global response is in the elastic regime and the properties of the structural system remain constant over time, the modal superposition principles allow decoupling the system of equations (1) into N independent equations [28]:

$$\ddot{Y}_j(t) + 2w_j \xi_j \dot{Y}_j(t) + w_j^2 Y_j(t) = f_j(t) \quad (2)$$

For a given vibration mode j , $Y_j(t)$, $\dot{Y}_j(t)$ and $\ddot{Y}_j(t)$ are the modal coordinates time histories for each of the N degrees of freedom associated with displacements, velocities and accelerations, respectively. In addition, w_j is the natural frequency related to the j^{th} vibration mode, while ξ_j is the damping coefficient, both modal values that do not change over time. On the loading side, the column matrix of nodal forces f_j results from the axle loads applied on the rails. Regarding the first part of equation (2), the modal structural values are not load-dependent (i.e., w_j and ξ_j), which allows only the definition of f_j to be required to compute the modal coordinates for each instant t , with these nodal forces calculated using simple linear shape functions by implementing the moving loads approach.

Naturally, the modal superposition principles may be considered to efficiently compute fatigue quantities such as stresses, strains or energetic parameters. Superimposing a limited number of vibration modes, the calculation of a certain value, ψ , may be expressed generically as:

$$\psi(t) = \psi_{sw} + \sum_j \psi_j Y_j(t) \quad (3)$$

where, ψ_{sw} is the permanent part of ψ and ψ_j is the respective modal quantity computed taking into account the modal shape of the j^{th} vibration mode.

For global fatigue analyses, nominal stress measures are required as input for predefined S-N curves, following the applicable normative specifications. According to EN1991-2 [29], such nominal quantities have to be properly amplified by the enhancement factors φ' and φ'' , with the former related to the effect of the moving trains and the latter associated with the influence of the irregularities of the track and vehicles imperfections. Assuming the average fatigue effects over 100 years, as normatively defined, a given nominal stress may be calculated as follows:

$$\sigma_{(\varphi)}(t) = \sigma_{sw} + \sigma_{sta} \cdot [1 + 0.5(\varphi' + 0.5\varphi'')] \tag{4}$$

in which, $\sigma_{(\varphi)}$ is the stress measure properly amplified and σ_{sta} is the static stress derived from the railway loading. Concerning φ' and φ'' , calibrated formulae are proposed in EN1991-2 [29]. Nonetheless, in the scope of dynamic analyses based on the moving loads approach, φ' can be specifically defined for the investigated case study, reducing overly conservative approximations:

$$\sigma_{(\varphi)}(t) = \sigma_{sw} + \sigma_{sta} \cdot [1 + 0.5(\sigma_{dyn}/\sigma_{stat} + 0.5\varphi'')] \tag{5}$$

where, φ' is the dynamic quantity divided by its static value, $(\sigma_{dyn}/\sigma_{stat})$, with the dynamic measure obtained from the term related to the modal superposition, $\sum_j \sigma_j \cdot Y_j(t)$, adapted from equation (3). Regarding φ'' , as alternative to the normative definition, a calibration process with a basis on the real profile of the irregularities of the existing track may be carry out, after performing representative calculations by implementing a bridge-train interaction methodology [30], doubly comparing these benchmark results with the values obtained for the moving loads approach and subsequently with the respective static outcomes. Finally, combining equations (4) and (5), the nominal stress of interest may be computed as follows:

$$\sigma_{(\varphi)}(t) = \sigma_{sw} + \left(\sum_j \sigma_j \cdot Y_j(t) \right) / (1 + \varphi') \times [1 + 0.5(\varphi' + 0.5\varphi'')] \tag{6}$$

As defined in EN1993-1-9 [7], the previous equation allows obtaining a certain fatigue loading to be associated with a fatigue strength defined by a given S-N curve, dependent on the investigated detail.

For local fatigue analyses, the implementation of reliable submodelling relations is critical to achieve numerical results in line with the structural response of the real mechanism of loading transference.

2.2 Submodelling techniques involving modal quantities

The reliability of the determination of stress and strain ranges and ultimately of fatigue damage predictions is related to the quality of the modelling. Logically, the increased complexity of structural systems leads to significant modelling works. Numerically, the accurate evaluation of local quantities in fatigue-critical details of bridges is a complex task that implicitly comprises an unavoidable multiscale problem. Generally, the global numerical model of a large structure is able to properly reproduce the global dynamic behaviour, even when conceived with beam or shell finite elements discretised with coarse meshes [4,9]. However, despite the accuracy of the global results, a local fatigue analysis demands a much more refined modelling approach, typically based on shell or volumetric finite elements, which tends to be hard to achieve through the inclusion of such a refinement directly into the global model, as it may significantly increase the computational costs. Nevertheless, for certain ranges of analysis, successful applications of this modelling method can be found in the literature [31–34]. An alternative effective approach consists in the analysis of the global model by computing the boundary displacement fields then imposed on the limits of a given refined local model, establishing a submodelling relation, with different techniques being available for computationally efficient applications [4,9,12]. Among them, those based on beam-to-shell, shell-to-solid and beam-to-solid relations should be highlighted, as they allow the combination of a lighter global model with refined local ones. Aiming local stress analysis and subsequent fatigue assessment, the implementation of submodelling techniques is critical, with the respective efficiency being leveraged by modal superposition concepts. The definition of the dynamic response with a basis on the latter theoretical concepts is affected by the existence of local nonlinearities related to contacts, with these influencing the type of modal quantities considered to perform the modal superposition. When no normal or friction contacts are involved, local values of interest may be computed adapting equations (4) to (6), superimposing the related modal quantities if the



a) partial perspective of the trussed structure



b) partial perspective of the ballastless track

Fig. 2. General view of the Várzeas Bridge (site photos).

response at the hot-spot is linear and time-invariant. This calculation strategy makes it possible to implement submodelling techniques based on modal boundary conditions ($BDCOs_j$), which then allow the necessary local modal quantities (y_j) to be calculated, with this approach being highly efficient [4,26]. On the other hand, for local responses influenced by contacts, the submodelling relation have to be established in the time domain, requiring the modal superposition of boundary conditions using equation (6) rewritten accordingly:

$$BDCOs_{s(\varphi)}(t) = BDCOs_{s_{sw}} + \left(\sum_j BDCOs_j \cdot Y_j(t) \right) / \left[(1 + \varphi^+) \times [1 + 0.5(\varphi^+ + 0.5\varphi^-)] \right] \tag{7}$$

where, $BDCOs_{s(\varphi)}$ are the amplified boundary displacement fields to be input into the submodel and $\sum_j BDCOs_j \cdot Y_j(t)$ is the term adapted from equation (3). For each train, for each time step, the $BDCOs_{s(\varphi)}$ may be imposed on a given and related local model to compute the required local stress time histories. Regardless of the different computational efficiencies, the local approaches that differ in their strategy to perform the modal superposition should allow the implementation of local fatigue methods [4,27].

3. The Várzeas Bridge case study

Following the objectives of the current work, a certain fatigue-critical detail of a structure located in Portugal was investigated by adopting several modelling scales properly related, as in the workflow outlined in Fig. 1. The Várzeas Bridge is composed of a riveted metallic structural system built in 1958, part of the international railway line of Beira Alta, which links Portugal to Spain (Fig. 2).

The structure has a total length of 281 m divided into three central spans of 60 m and two extreme ones of 50.50 m. Concerning the typology of the structural system, different groups of elements may be defined: (i) two inverted Warren trusses are connected by cross-girders, materialising the deck and supporting the ballastless railway track; (ii) three different levels of longitudinal bracings connecting the longitudinal elements (inferior, superior and noising bracings); (iii) the cross-sectional bracings are regularly spaced and connected to the inferior flanges, vertical-posts of the inverted Warren trusses and cross-girders; (iv) four trapezoidal shape trusses of different heights act as columns; and (v) one granite masonry column (on the west side) and one granite masonry abutment (on the east side) also support the railway loadings. In addition, on the west side, a 20 m long simply supported span links the railway station of Luso to the Várzeas Bridge.

Regarding the main dimensions of the structural system, the two inverted Warren trusses are 5.95 m high and 4.40 m wide, with the first and last five girder panels being 6.50 m long and the remaining ones of 6.00 m ($5 \times 6.50 \text{ m} + 3 \times 6.00 \text{ m}$ in the extreme spans). Also, the metallic columns have different heights between 10.10 m and 30.20 m and that composed of granite masonry is 12.20 m tall.

The superior flanges of the inverted Warren trusses are composed of two U-shaped sections of 400 mm in height, connected by a continuous plate 650 mm wide and 12 mm thick. The inferior flanges have a similar geometry, but such a plate is 13 mm thick, which increases to 20 mm close to the columns (6 m on each side). Regarding the diagonals, a general cross-section was found, composed of two U-shaped sections of 350 mm in height, being modified at the truss panels close to the columns to a cross-section defined by two U-shaped sections of 400 mm in height. The vertical-posts have an I-shaped cross-section with 348 mm in height and 297 mm in width, modified to an I-shaped section with 348 mm in height and 560 mm in width at the connections truss-to-column. The cross-girders

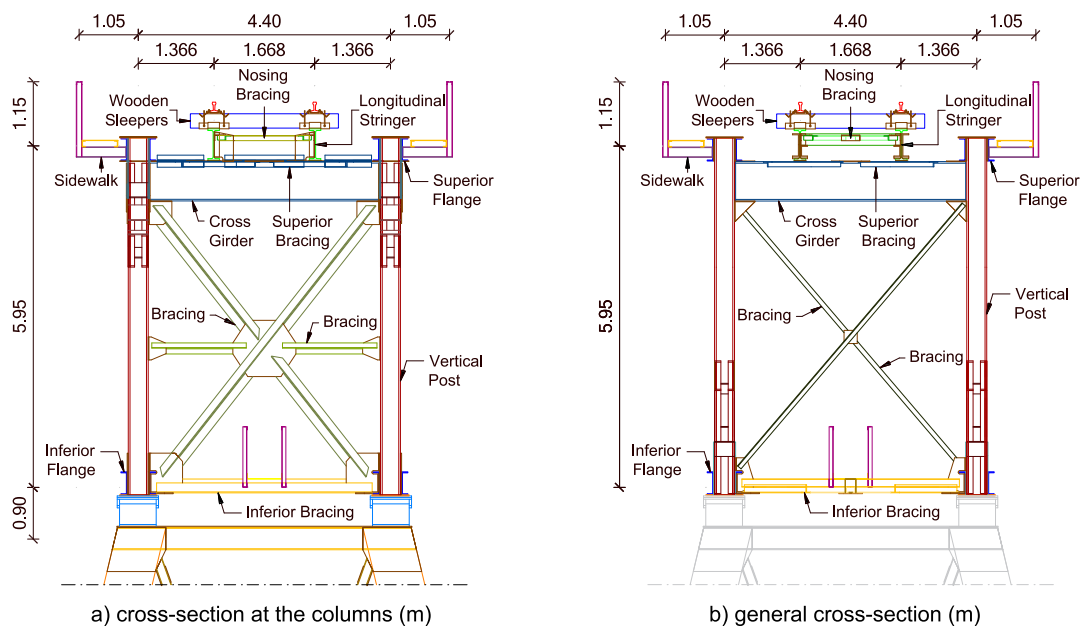


Fig. 3. Cross-sections of the Várzeas Bridge (schematic drawings).

support the longitudinal stringers under the track, both composed of I-shaped sections, the former of 688 mm in height and 297 mm in width and the latter of 550 mm in height and 200 mm in width. Also, the cross-sectional bracings and the three levels of longitudinal bracings (inferior, superior and nosing bracings) are composed of L-shaped, half I-shaped or U-shaped sections (Fig. 3).

The number of confluent structural members at certain nodes leads to connections of considerably complex geometry. Numerous angles and filling plates, with a general thickness of 14 mm, are used to establish and level the union between line elements. Also, a large number of rivets was found, with two different ranges for the nominal diameter: (i) 22 mm to 32 mm for connections between the most important structural elements (truss flanges, diagonals, vertical-posts, cross-girders and longitudinal stringers); and (ii) 9 mm to 20 mm for the remaining details involving bracing members (Fig. 4).

The metallic bearing supports allow free rotations on the longitudinal plane. On the west side, the longitudinal displacement is also free, allowing to accommodate movements caused by horizontal forces, e.g., thermal loading, traction and braking forces. On the other hand, at the remaining supports, the longitudinal displacement is constrained. Nevertheless, due to the flexibility of the metallic columns, the east abutment absorbs the majority of forces caused by horizontal deformations.

3.1 Development of the global model

As shown in Fig. 1 in i), the evaluation of the structural integrity should be initiated by conceiving a global model able to reproduce the responses at the global scale. In Civil Engineering, the types of elements to be considered are largely influenced by the complexity and length of structural systems, namely by the number of members and size. In general, depending on the structural typology and characteristics, beam and shell elements are reasonable options to build global models.

The multiplicity of line elements and respective connections gives the structural system of the Várzeas Bridge a considerable complexity, which has relevant implications in the structural analysis, but also in any numerical modelling to be conceived. In addition, as previously described, the variability of the girder panels geometry, the different bracing levels and the complexity of the nodal connections lead to the necessity of adopting a careful numerical modelling approach to capture accurately the global and local dynamic behaviour of the bridge. Therefore, taking into account the described structural complexity of the Várzeas Bridge, as well as the considerable length, it seemed reasonable to conceive a global model using beam elements. Naturally, such a modelling approach was built assuming an adequate detail to reproduce with sufficient accuracy the global dynamic behaviour, using ANSYS software [35] (Fig. 5).

Beam elements (BEAM188 [36]) were applied to model all the metallic elements that compose the structural system of the Várzeas Bridge (deck and columns). Rails and wooden sleepers, part of the ballastless railway track, were explicitly modelled considering BEAM188 elements as well. Additionally, spring-damper elements (COMBIN14 [36]) were used to numerically represent the elastic stiffness of the metallic pads between the rails and the wooden sleepers and between the wooden sleepers and the longitudinal stringers. Also, COMBIN14 elements were employed to model the stiffness of the foundation of the metallic columns. Nodal mass elements (MASS21 [36]) were used to account for the mass of the rivets, filling plates and non-structural elements, e.g., sidewalk and deck inspection access. Lastly, in order to connect the centre of gravity of the beam elements modelling the railway track, rigid connections (MPC184 [36]) were applied.

3.1.1. Geometrical and material characteristics

In the present subsection, the geometrical and material properties of relevant structural elements that compose the bridge are characterised and described, as considered in the modelling. Concerning the cross-sectional characteristics, the most important mechanical properties are presented, such as the gross area, A , and the local inertias according to the assumed local axis, I_y and I_z . Nonetheless, it should be noted that the parameters related to the torsional behaviour were evaluated and properly assumed, with the aim of accurately representing the local characteristics at the member scale. Regarding the nodal connections, representative local models were conceived and investigated under static loading, with such an information, as well as the characterisation of the remaining structural members, presented in detail in [4], assuming that the respective full presentation would make the present work unnecessarily extensive.



a) nodal connection with confluent diagonals



b) nodal connection at a column

Fig. 4. Cross-sections of the Várzeas Bridge (site photos).

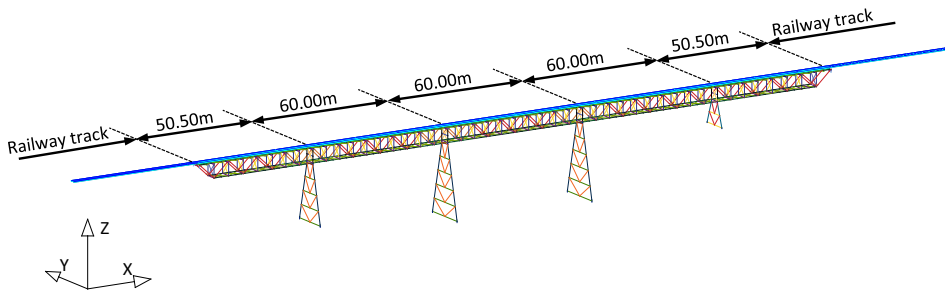


Fig. 5. Numerical model of the Várzeas Bridge (global view, schematic representation) (global scale).

a) Inverted Warren trusses

The inferior and superior flanges, diagonals and vertical-posts, which are critical members of the structural system that supports longitudinally the dead loads and remaining variable loadings, compose the two inverted Warren trusses. The geometrical characteristics attributed to such structural elements and the local axis systems adopted are summarised in Table 1.

Despite the age of the bridge, the material that composes the structural members is expected to have characteristics of a typical modern structural steel. The results achieved in material tests carried out on samples of the Trezói Bridge, located on the same line and built by the same contractor at the same period, were assumed as a reference to justify such an option [37]. For the main structural elements, the St52 grade defined in the original design information is assumed as the S355 modern structural steel grade [38]. Therefore, a Young’s modulus, E , of 210 GPa, density, ρ , equal to 7850 kg/m³, yielding stress, f_{yd} , of 355 MPa and a Poisson’s ratio, ν , equal to 0.27 were adopted.

b) Cross-girders and longitudinal stringers

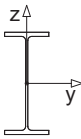
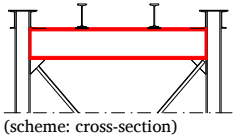
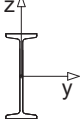
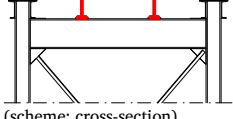
The two inverted Warren trusses are connected by the cross-girders that support the longitudinal stringers, which support the ballastless railway track (rails, sleepers and pads). These structural elements compose a structural subsystem that contributes for the global behaviour and is associated with relevant local responses. The geometrical characteristics attributed to the cross-girders and longitudinal stringers are summarised in Table 2.

Also, for the cross-girders and the longitudinal stringers, the St52 originally specified was assumed as the S355 steel grade, adopting the same mechanical characteristics associated with modern steel, as for the members of the inverted Warren trusses. The cross-girders connected to these latter elements compose the part of the structure that supports and distributes the railway loading to the supports, assuming a critical role for the load-carrying capacity of the bridge.

Table 1
Geometrical characteristics of the cross-sections: inverted Warren trusses.

Section	Location	Properties
Inferior flange general section 2 UPN400 + 13 mm Flange	<p>(scheme: side view)</p>	$A=2.675 \times 10^{-2} \text{ m}^2$ $I_y=6.537 \times 10^{-4} \text{ m}^4$ $I_z=1.114 \times 10^{-3} \text{ m}^4$
Superior flange 2 UPN400 + 12 mm Flange	<p>(scheme: side view)</p>	$A=2.610 \times 10^{-2} \text{ m}^2$ $I_y=6.392 \times 10^{-4} \text{ m}^4$ $I_z=1.136 \times 10^{-3} \text{ m}^4$
Diagonal at columns 2 UPN400	<p>(scheme: side view)</p>	$A=1.830 \times 10^{-2} \text{ m}^2$ $I_y=4.071 \times 10^{-4} \text{ m}^4$ $I_z=4.136 \times 10^{-4} \text{ m}^4$
Vertical-post at columns (560 × 30) × (348 × 25) mm	<p>(scheme: side view)</p>	$A=4.080 \times 10^{-2} \text{ m}^2$ $I_y=8.785 \times 10^{-4} \text{ m}^4$ $I_z=9.017 \times 10^{-4} \text{ m}^4$

Table 2
Geometrical characteristics of the cross-sections: cross-girders and longitudinal stringers.

Section		Location	Properties
Cross-girder (688 × 28) × (297 × 15) mm		 (scheme: cross-section)	$A=2.674 \times 10^{-2} \text{ m}^2$ $I_y=2.188 \times 10^{-3} \text{ m}^4$ $I_z=1.226 \times 10^{-4} \text{ m}^4$
Longitudinal stringers (550 × 30) × (200 × 19) mm		 (scheme: cross-section)	$A=2.121 \times 10^{-2} \text{ m}^2$ $I_y=9.899 \times 10^{-4} \text{ m}^4$ $I_z=3.488 \times 10^{-5} \text{ m}^4$

3.2 Optimisation of the global model

Conceiving numerical models requires inevitably assumptions and simplifications, which may directly influence the numerical dynamic characteristics and structural performance. The uncertainties about the properties of the model may be reduced by implementing optimisation methodologies, comparing the numerical and experimental modal results and iteratively minimising the existing errors [39].

Concerning the Várzeas Bridge, two different tests were carried out, which are recommended for similar structural systems: (i) a global Ambient Vibration Test (AVT), focused on evaluating the modal dynamic properties associated with the global behaviour of the structural system, mainly related to the truss chords, diagonals, vertical-posts and cross-girders; and (ii) a localised AVT, conceived to characterise the response of the identified structural subsystem, associated with the ballastless railway track, including the longitudinal stringers. Such *in situ* experimental tests were performed as completely independent tasks and were planned to investigate different ranges of frequencies and respective modal shapes.

As advised, the global AVT was performed, covering the full length of the structure by monitoring a total of 58 points in 3 directions (refer to Fig. 6): (i) vertical, zz; (ii) transversal, yy; and (iii) longitudinal, xx. Due to the limited number of available sensors, 9 different setups were performed. The results of each test configuration were related to each other using 3 reference points (RP), 2 monitoring

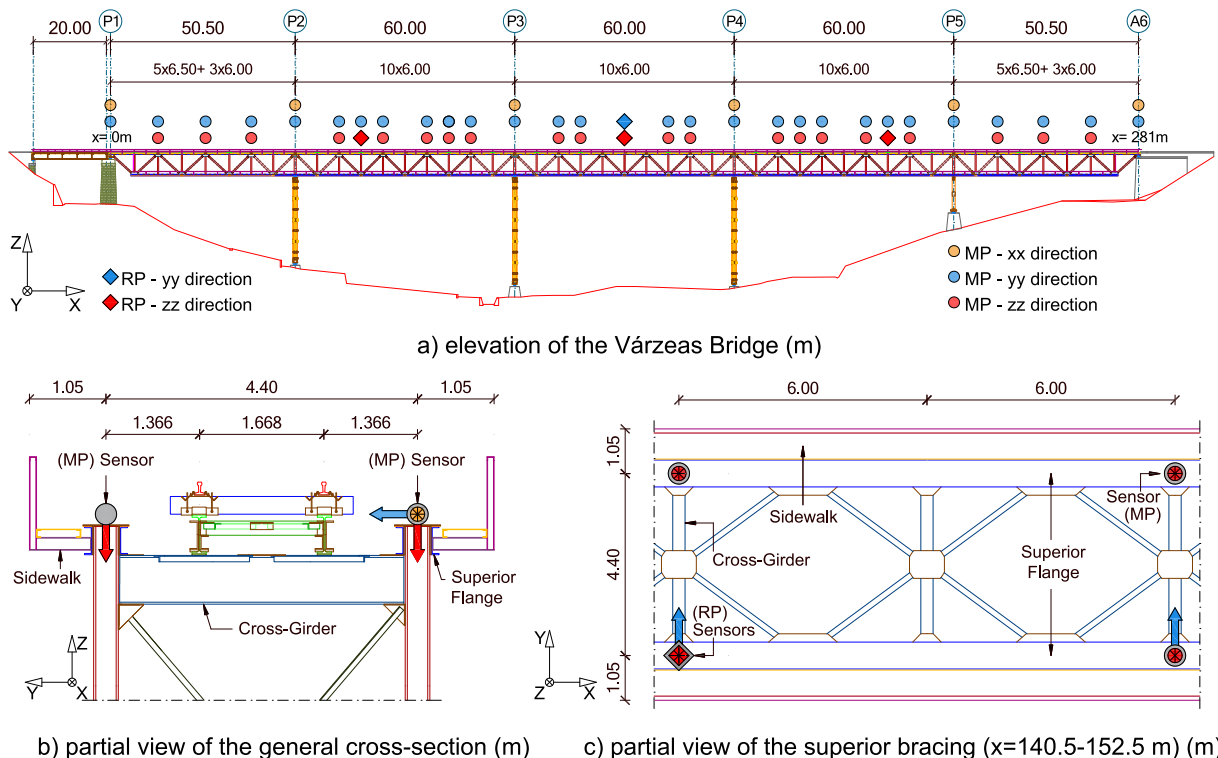


Fig. 6. Global AVT: monitoring directions and measurement points.

exclusively the vertical direction and 1 monitoring the vertical and transversal directions simultaneously; 55 mobile points (MP) were considered.

In Fig. 6, the monitoring directions and measurement points, located on the superior flange of the inverted Warren trusses, are identified. The accelerometers used to evaluate the transversal direction were placed only on one side, as the compatibility of displacements between both Warren trusses was verified in this direction due to the high axial stiffness of the cross-girders (Fig. 6 b) and c)).

Regarding the sensors, 16 piezoelectric accelerometers (PCB 393B12) with a high sensitivity of 10 V/g were used to record accelerations in the range of ± 0.5 g and in the frequency interval between 0.15 Hz and 1000 Hz. Data acquisition was performed using a National Instruments cDAQ-9188 system with NI9234 IEPE input modules. The time series were acquired over 10-minute periods, considering a sampling frequency of 2048 Hz posteriorly decimated to 256 Hz. Due to the length of the Várzeas Bridge, coaxial cables up to 150 m were used to connect the accelerometers to the data acquisition hardware, placed at the central point of the structure (Fig. 7).

The data acquired during the 9 setups were processed using the EFDD algorithm available in Artemis software [40]. 18 vibration modes with different configurations were clearly identified, namely, transversal (yy-direction), pure bending (zz-direction) and torsion vibration modes.

Focused on the investigation of the identified structural subsystem, the localised AVT is advised and it was performed, covering 30 m in length by monitoring a total of 42 points in the vertical direction, zz. The restrictions in terms of available sensors led to the implementation of 5 different setups, related to each other using 5 reference points (RP); 37 mobile points (MP) were considered.

In Fig. 8, the measurement points on the webs of both longitudinal stringers are identified. 21 monitoring points spaced of 1.5 m were located to capture the vertical and torsion vibration modes. Also, a reference accelerometer placed on the superior flange of one Warren truss was considered to distinguish the localised vibration modes from the global ones.

Concerning the sensors and data acquisition hardware, the same equipment used in the global AVT was used. Also, coaxial cables up to 20 m were used to connect the piezoelectric accelerometers to the data acquisition system, placed at the central point of the 30 m covered by the AVT (Fig. 9).

As for the global AVT, the experimental values acquired during the 5 localised setups were processed using the EFDD algorithm available in Artemis software [40]. 10 vertical vibration modes with different shapes were clearly identified.

Once the experimental data was defined, an optimisation methodology using a genetic algorithm was implemented to minimise the difference between experimental and numerical modal properties, considering the energy modal assurance criterion (EMAC) to improve the mode pairing [41,42]. As variables of the problem, several geometrical and material properties were assumed to be related to uncertainties and their optimal values were searched [4]. The first optimisation phase focused on the localised modes of the structural subsystem associated with the ballastless railway track (Fig. 10).

In Fig. 10, the results of the mode pairing after the optimisation are presented. An average error in terms of frequency, $\overline{\Delta e_f}$, of 1.507% was achieved, as well as an average modal assurance coefficient, \overline{MAC} , equal to 0.948. Also, from the initial value of 0.996, the result for the objective function was minimised to 0.670. In general terms, the numerical modelling of the identified subsystem is an accurate numerical representation of the real structural behaviour after the optimisation, with the mass of the wooden sleepers influencing greatly the localised modes. In addition, the optimisation of the geometrical and material properties related to uncertainties that influence the global response was carried out (Fig. 11).

In Fig. 11, the mode pairing is presented after the optimisation. Similar to the localised results, a good agreement was achieved between experimental and numerical values ($\overline{\Delta e_f}=2.995\%$ and $\overline{MAC}=0.949$). Also, the value of the objective function was minimised from 1.595 to 1.467. Overall, the stiffness of the metallic connections related to the inverted Warren trusses and cross-girders was optimised, influencing the results obtained, with the mass of the wooden sleepers also relevant for the global modes.

Considering the outcomes achieved after the two optimisations performed (localised and global), the 28 vibration modes experimentally assessed and the corresponding numerical values, the following quantities were obtained: (i) $\overline{\Delta e_f}$ equal to 2.464%; (ii) \overline{MAC} of 0.948; and (iii) a minimum value for the objective function equal to 2.137. Therefore, the global model may be considered as an accurate numerical representation of the real structure.

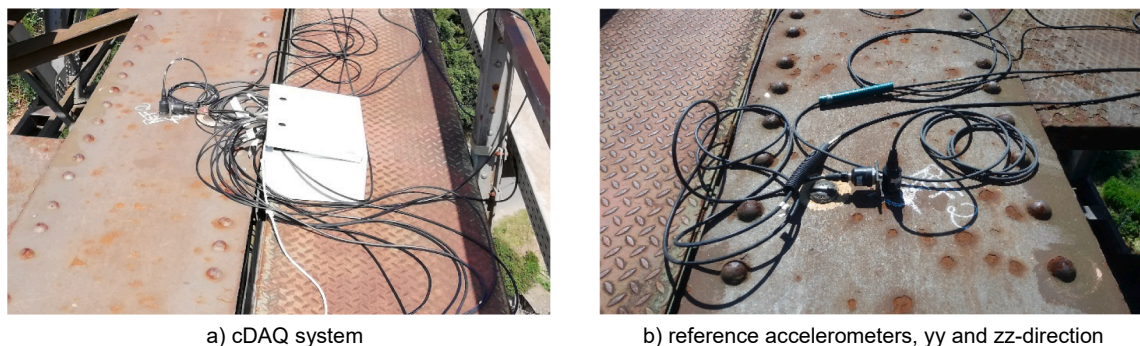


Fig. 7. Global AVT: sensors and data acquisition system.

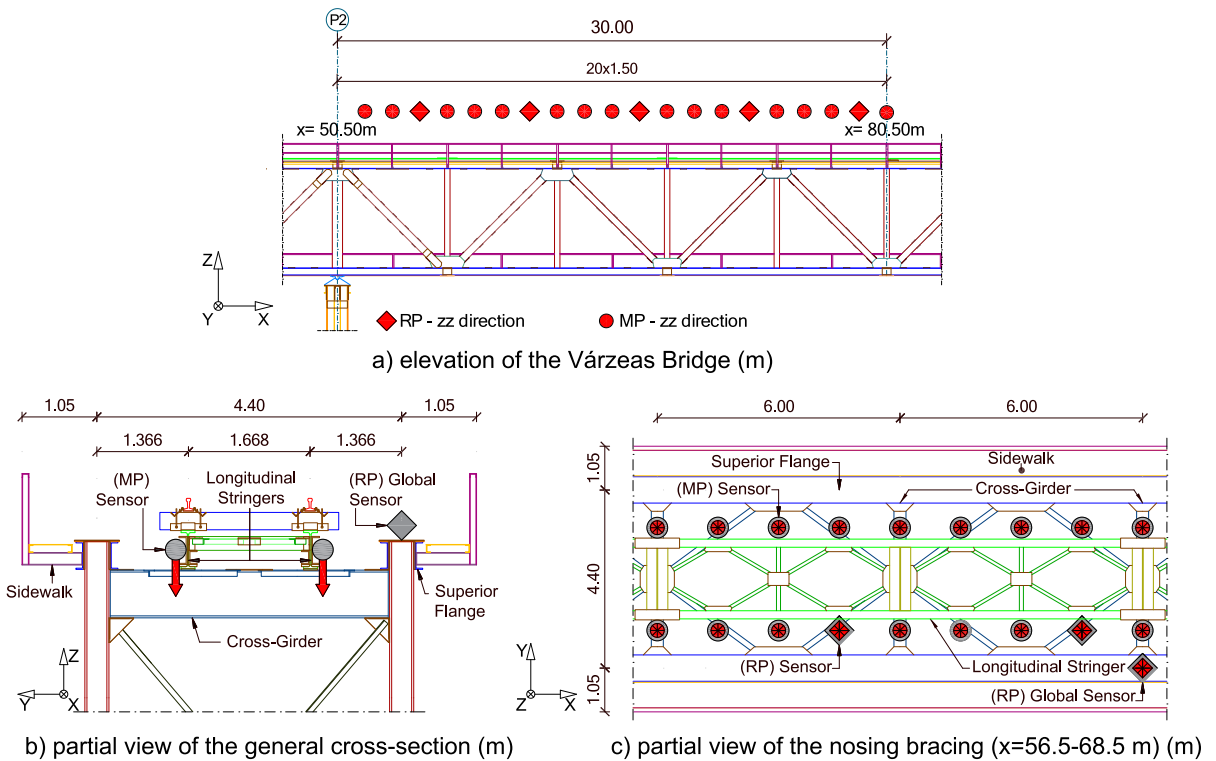


Fig. 8. Localised AVT: monitoring directions and measurement points.

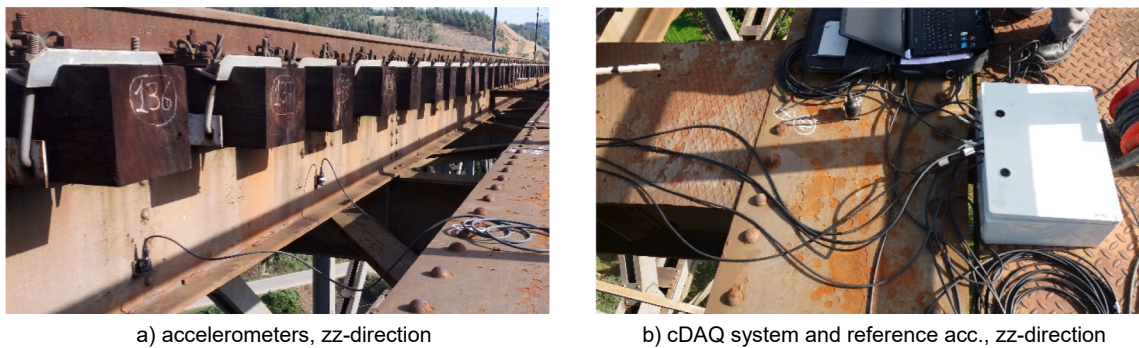


Fig. 9. Localised AVT: sensors and data acquisition system.

3.3 Fatigue analysis by implementing a global approach

Although this paper is oriented towards local stress evaluation, which can be explored in local fatigue assessment approaches, following the flowchart presented in Fig. 1, the global fatigue analysis was implemented, allowing the most critical details to be defined, with these calculations being briefly presented. The linear damage accumulation method proposed in EN1993-1-9 [7] to design new details may be considered to screen the existing fatigue-critical connections, after computing fatigue damage associated with a given railway traffic and assuming reasonable conservative assumptions. In the present work, the heavy traffic mix suggested in the applicable EN1991-2 [29] was assumed as first approach, taking into account the available data concerning the past and the present traffic. Thirteen types of riveted details were identified connecting the metallic structural members. All of them were analysed, performing quasi-static and dynamic calculations, with the respective outcomes being properly amplified according to the normative specifications [29] (equations (4) and (6), respectively), adopting the cross-sections net properties to compute the nominal stresses. After, the rainflow cycle counting method was implemented to define the nominal stress ranges, $\Delta\sigma_i$, and the associated number of cycles, n_i . Once obtained the $\Delta\sigma_i-n_i$ histogram, the fatigue life of a given detail when submitted exclusively to $\Delta\sigma_i$ was calculated and expressed in terms of cycles, N_i , assuming the appropriate S-N curve for nominal stresses. In this regard, the applicable EN1993-1-9 [7] does not provide any guideline for riveted details. Nonetheless, several researches have been proposing the detail category 71 as a

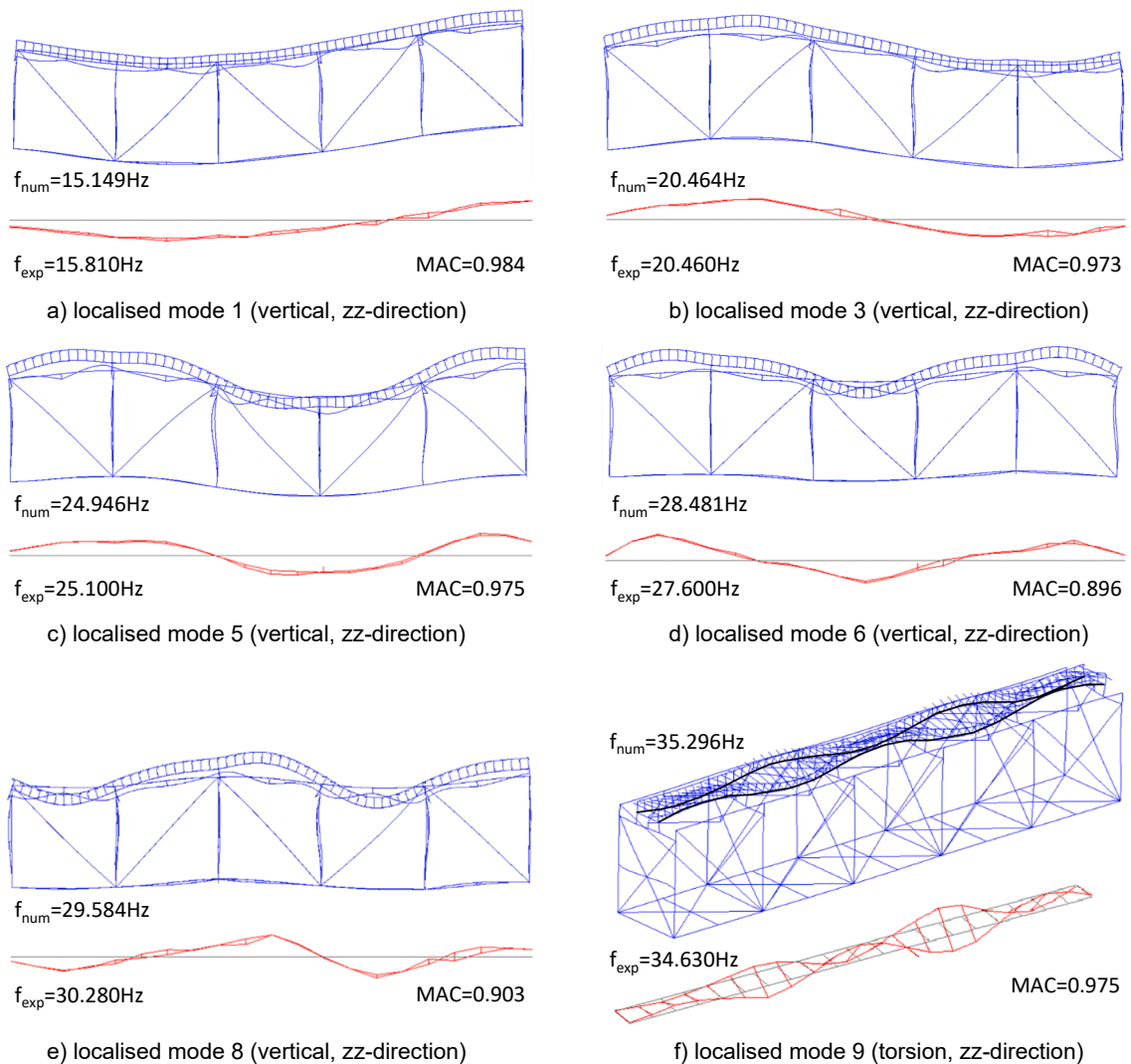


Fig. 10. Localised modes: experimental vs. numerical vibration modes.

lower bound to analyse such a type of connection, and this resistance limit was then assumed to identify the critical details. After evaluating 2286 connections, the details associated with the diagonals were found to be the most critical to fatigue, requiring a subsequent local analysis. Representatively, the riveted connection of the diagonal to the gusset plates located at $x=109.30$ m, and part of the node at $x=110.50$ m, was investigated by establishing a validated submodelling relation properly addressing the existing geometrical, material and contact nonlinearities to evaluate the local stress time-histories of interest.

4. Refinement of the global model

As said, for large structures, global models must be conceived to obtain an accurate numerical representation of the global structural responses, allowing efficient calculations compatible with the pace and deadlines associated with Civil Engineering tasks. However, for fatigue-critical connections identified by applying global methods, more accurate calculations must be carried out. As shown in Fig. 1 in ii), an improved modelling of the structural members associated with a certain detail of interest should be conceived to relate the outcomes obtained at the global and local scales.

4.1 Local shell modelling

In order to investigate large bridges, a progressive modelling should be adopted, from the global scale, defined using line elements, to the local one, characterised with solid elements. The incorporation of shell refinements on the global model is assumed as an intermediate modelling scale that, combined with the experimental validations, allows achieving a submodelling relation with the local

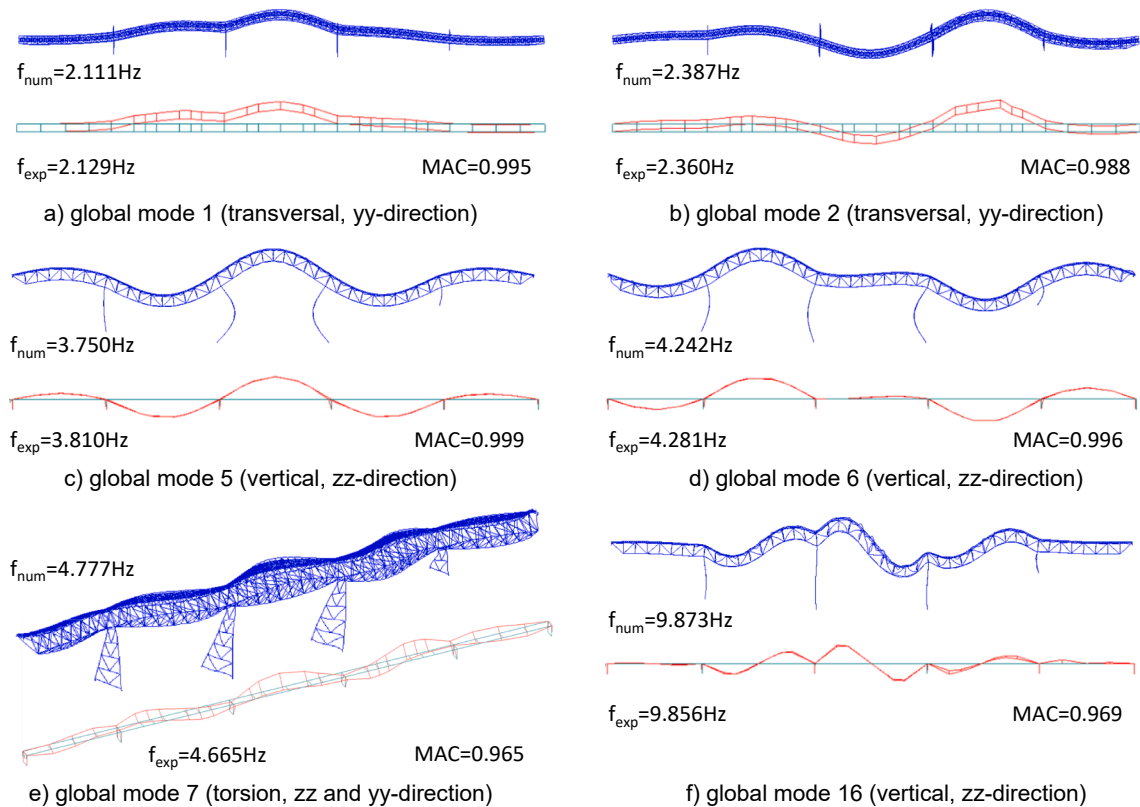


Fig. 11. Global modes: experimental vs. numerical vibration modes.

solid model more in line with the real structural response. When it is not computationally admissible, an intermediate submodel at the member scale may be conceived using shell elements (see Fig. 1).

Among the connections with higher fatigue damage, those associated with the diagonals were preferentially analysed due to their importance for the global structural behaviour and lack of redundancy. If any of those riveted details is affected by relevant fatigue damage, the load-carrying capacity of the structural system is compromised. Thus, in order to investigate the connection at $x = 109.30$ m related to the diagonal, part of the superior node at $x = 110.50$ m, a refinement of the model between $x = 98$ m and $x = 113$ m, was performed, improving the modelling at the member scale. Shell finite elements were considered to numerically represent the members of the main structural system and longitudinal stringers. On the other hand, the bracing systems, rails and sleepers were defined by beam finite elements, as in the previous version of the global model. Furthermore, it should be stressed that the positions of the inferior and superior flanges of the inverted Warren trusses were assumed as reference to conceive the planned refinement at the member scale (Fig. 12).

In Fig. 12, the shell refinement of the length between $x=98$ m and $x=113$ m is presented. The incorporation of the conceived modelling enhancement, essentially based on shell finite elements, into the existing global model composed of beam finite elements was carefully defined to minimise local distortions and geometrical nonlinearities, refer to Fig. 13.

Part of the links between the shell and beam elements and the non-modified members of the global model are outlined in Fig. 13. Two different techniques were considered: (i) beam-to-shell links based on multi-point constraint equations, in which the nodal forces acting at the extreme node of a certain beam are distributed to the nodes of the corresponding shell finite elements according to the respective position, i.e., a relation *master-slave* was defined; and (ii) beam-to-beam links, in which the nodal forces are directly transmitted between the nodes of different line elements, resulting in the merging of the *DOFs* of the connected nodes. After incorporating the shell refinement into the global model, a modal analysis was performed to verify if any significant change would be obtained, and no relevant modifications were identified for the 28 numerical vibration modes previously associated with those identified experimentally (see Figs. 10 and 11).

4.2 Validation of the refined global model

In order to ensure a high level of accuracy and a high degree of confidence compatible with the computational effort and refinement of the modelling performed, it is necessary to evaluate whether the refined global model is able to adequately reproduce the time histories of stresses assessed in the real structure. For this purpose, a short-term experimental campaign was carried out to evaluate the

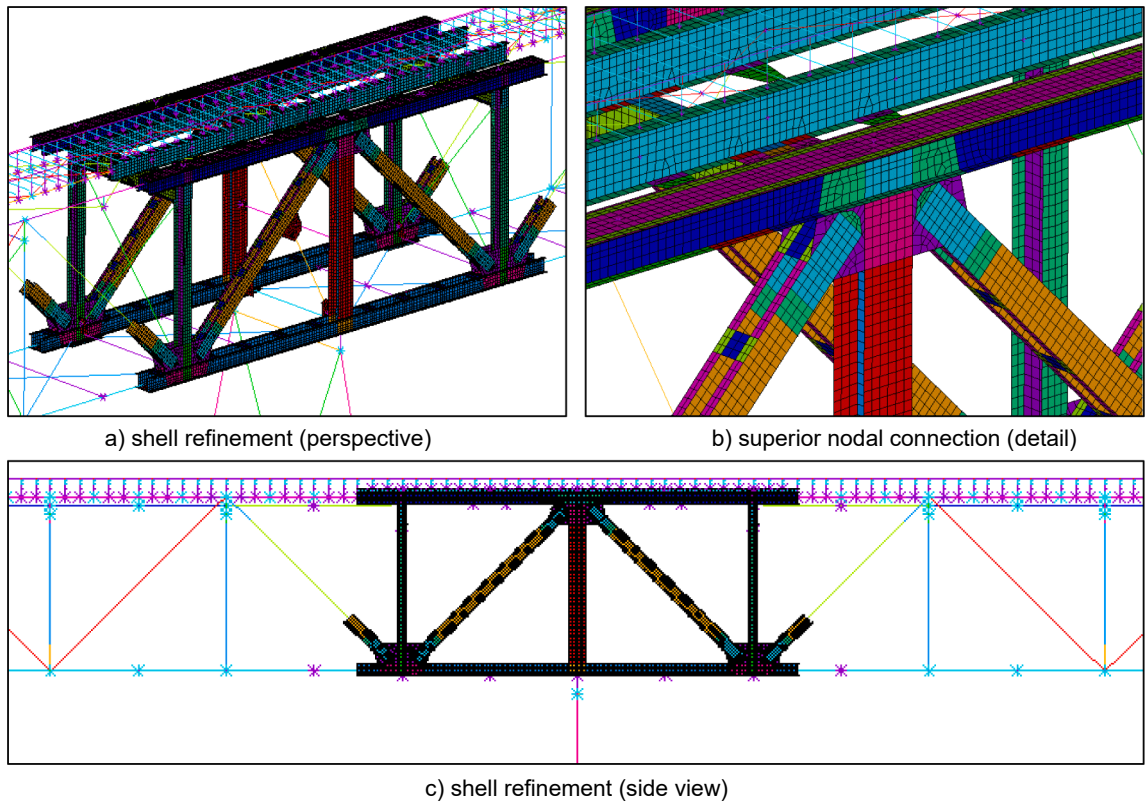


Fig. 12. Refinement incorporated into the global beam model (member scale).

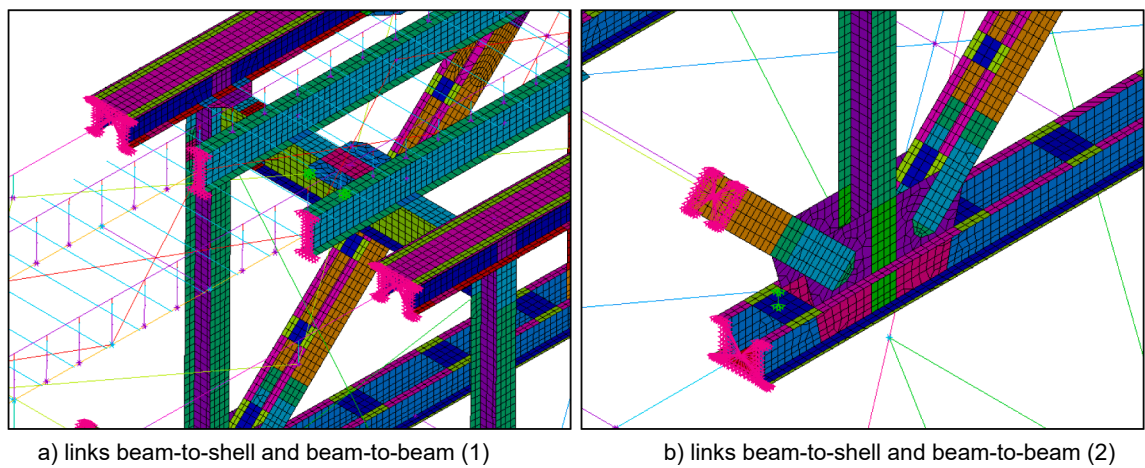


Fig. 13. Shell modelling and respective links to the global model (member scale).

strains (strain gauge sensors) and associated stresses at positions of interest, originated by a given train with known axle loads. No weighing campaign was performed in the scope of this work and regular passenger trains were taken into account for such an assessment.

Considering the numerical results previously obtained, as well as the geometry in the vicinity of the critical detail, the position of each strain gauge was planned to evaluate the strain measurements at 19 points located on the different members. Two groups of experimental sensors were defined: (i) the strain gauges associated with the structural elements part of the nodal connection at $x = 110.50$ m; and (ii) the strain gauges related to the cross-girder and vertical-post at $x = 104.50$ m. 14 strain gauges were installed on the structural members associated with the nodal connection at $x = 110.50$ m, i.e., the cross-girder, the superior flange, the vertical-post and the diagonal (Fig. 14). Also, the remaining 5 strain gauges were installed at the positions associated with the cross-girder and the

vertical-post, part of the nodal connection without confluent diagonal at $x = 104.50$ m (Fig. 15).

In general, near to relevant riveted geometries, 3 sensors were installed by each cross-section with the aim of defining the stress plane from the obtained strain measurements. Also, other strain gauges were planned in order to evaluate additional strain time histories. *In situ* works associated with the installation of the strain gauges are shown in Figs. 16 and 17 for some of the positions at $x = 110.50$ m and $x = 104.50$ m, respectively.

In addition to the foreseen sensors for strain measurements, two redundant strategies were adopted to calculate and validate the speed of each train circulating on the bridge, namely: (i) two optical sensors were placed separated by a known distance; and (ii) two rail pad sensors were installed at different pre-established locations. In both cases, for each train, a time history of the respective measured quantity was evaluated, allowing to detect the passage of the axle loads and consequently to obtain the velocity of the trains in circulation with known distances between axles.

Regarding the data acquisition system, a National Instruments cRIO-9172 was adopted. Depending on the type of sensors installed, each of them was connected to an acquisition module to translate into structural parameters the recording of the respective quantities, e.g., through the relative variation of the electrical resistance or changes in the characteristics of the light beams. Concerning the 19 installed strain gauges, the connection was made to a National Instruments module NI 9236 (1/4 Wheatstone bridges), while the optical sensors were connected to a module NI 9239 and the adopted rail pad sensors were linked to a module NI 9237.

For two days, the strain time histories for several trains were evaluated. The circulation of three types of rail vehicles was recorded: (i) regional passenger trains; (ii) intercity passenger trains; and (iii) freight trains. Despite the relevance for fatigue damage of the latter, only the axle loads of the first two are typified and available in official information provided by the operating companies and in previous works in which weighing tasks were performed [43–45]. For this reason, such trains were considered to carry out the foreseen validation of the conceived and refined numerical model. Consequently, comparisons were made between the numerical stress time histories and the respective experimental values, indirectly obtained from the evaluated strains assuming a purely linear elastic behaviour for the material. The results for a regional passenger train with twelve axles of 115 kN in average, circulating at an average velocity of 53.34 km/h, are presented (Fig. 18).

In Fig. 18, the experimental and numerical stresses are compared for several strain gauges and an excellent agreement can be verified. Naturally, for a regional passenger train characterised by reduced axle loads, the magnitudes of the evaluated stresses were also found low. For the normative fatigue trains proposed in EN1991-2 [29], higher stress values are expected. In general, if the magnitude of the railway loading is compatible with the elastic regime, the numerical results are expected to be in accordance with the real structural responses. Overall, it can be concluded that the global model conceived using line elements and refined mainly with shell ones is able to properly reproduce the dynamic behaviour of the real structure. After validating the shell refinement, a further submodelling relation can be fully established in order to low the analysis scale to the rivets vicinity, accounting for the detailed geometry of the connection, taking advantage of the progressive modelling.

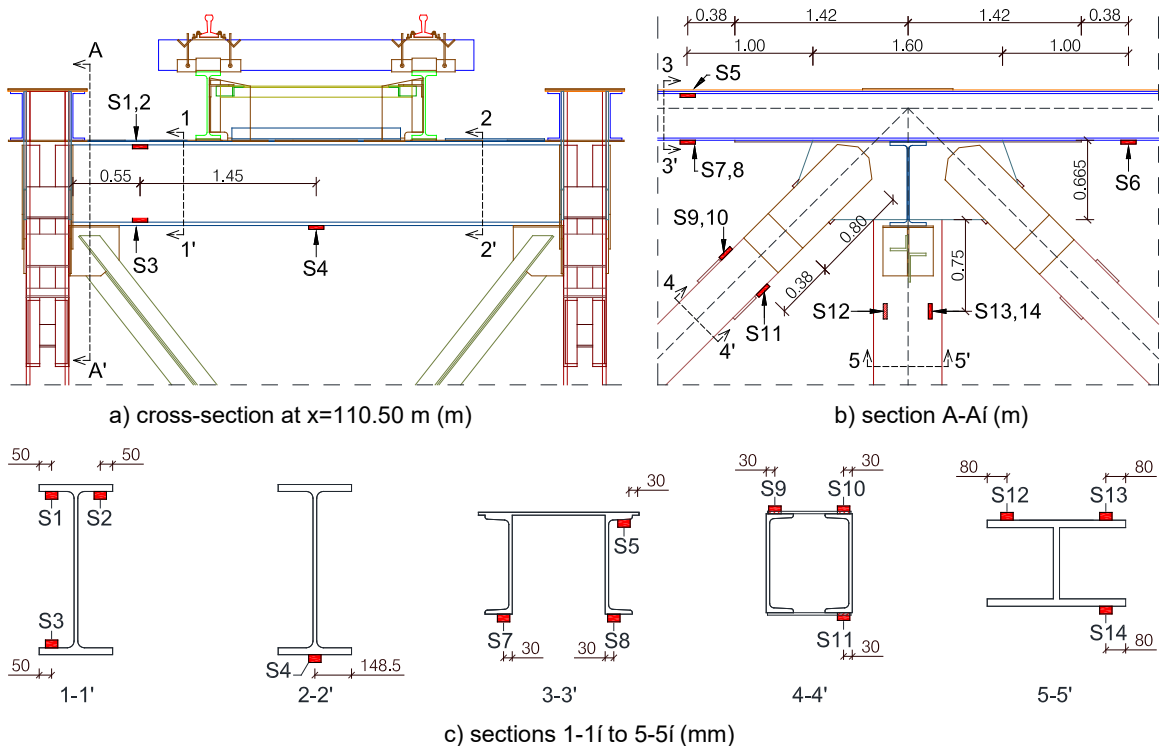


Fig. 14. Position of the strain gauges installed on the cross-sections at column P3 ($x=110.50$ m).

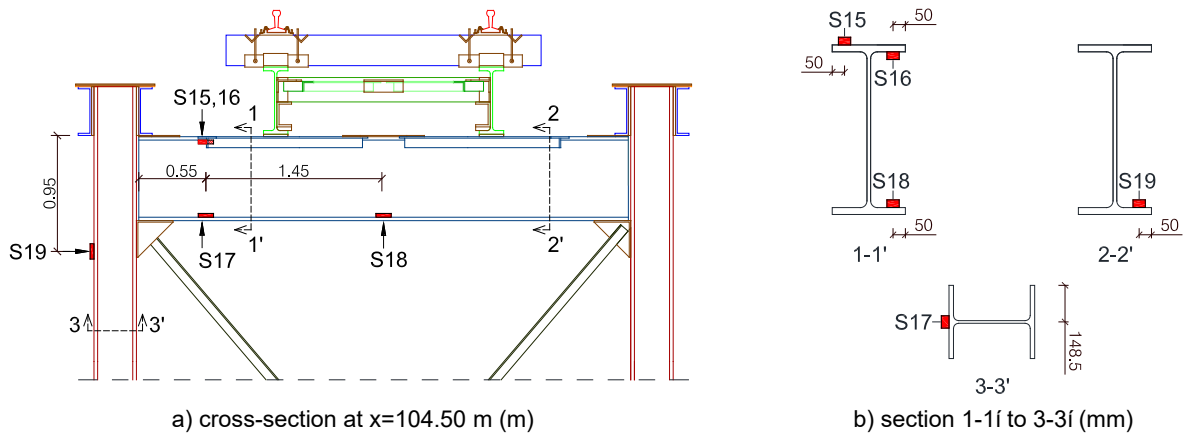


Fig. 15. Position of the strain gauges installed on the cross-sections close to column P3 ($x=104.50$ m).



a) S2 (before the mechanical protection)

b) S3 (before the mechanical protection)



c) S9 and S10 (after the mechanical protection)



d) S12 and S13 (after the mechanical protection)

Fig. 16. Strain gauges installed on the cross-sections at column P3 ($x=110.50$ m).

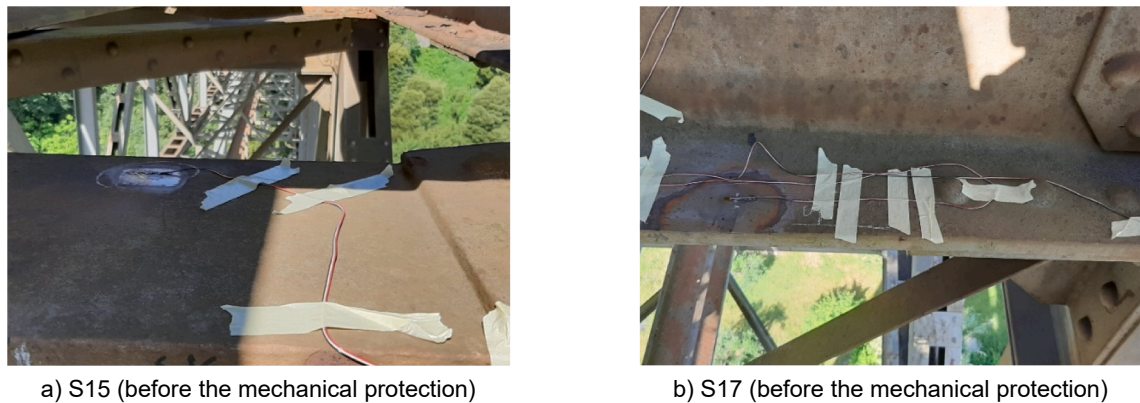


Fig. 17. Strain gauges installed on the cross-sections close to column P3 ($x=104.50$ m).

5. Advanced modelling based on a Global-Local relation

Once the global model has been optimised, refined and validated, it can be stated that the numerical responses at such a scale reflect the real structural behaviour, allowing to implement calibrated submodelling relations with detailed local geometries. As a consequence, the numerical structural responses at the local scale are expected to be identical to the real ones, in particular the local stress values that should lead to an accurate fatigue assessment, as foreseen in Fig. 1 in iii).

5.1 Development of the solid submodel

Considering the local geometrical and material properties, a solid submodel was developed to locally investigate the structural response of the fatigue-critical connection of interest. A local geometrical survey was performed, allowing to evaluate the dimension and thickness of the existing plates. Concerning the rivets, the corresponding locations were defined and the dimension of the respective heads was measured. After, the remaining geometrical characteristics, including the nominal diameter of the shaft, were defined as proposed by Åkesson [46]. Based on the evaluated information, the solid submodel of the riveted detail located at $x=109.30$ m was conceived, adopting mainly volumetric finite elements to replicate the real structure as accurately as possible (Fig. 19).

In Fig. 19, the conceived local model is presented and the respective structural members are identified. Due to the geometrical and loading symmetry of the bridge about the plane Oxz , as defined in Fig. 5, only the nodal connection at $x = 110.50$ m with higher global yy -coordinates was modelled to investigate the riveted detail at $x = 109.30$ m.

Two diagonals, each one composed of two UPN400 cross-sections, are connected to two gusset plates 14 mm thick. Additionally, two strengthening plates 14 mm thick on each side of each diagonal form a distributed mechanism of loading transference (inner and outer plates). Such components materialise several admissible loading paths, increasing the redundancy of the riveted connection. The superior flange, composed of two UPN400 and a continuous plate 12 mm thick, is connected to the gusset plates by the webs of the U-shaped sections. Concerning the vertical-post, the I-shaped cross-section that materialises it was modelled and linked to the gusset plates. Transversally, the cross-girder composed of an I-shaped section is connected through its web to the gusset plates using two L-shaped sections. Regarding the cross-sectional bracing, two L-shaped sections are linked to a corner plate 12 mm thick, connected to the inferior flange of the cross-girder and to the inner flange of the vertical-post. In addition, as part of a localised bracing over the columns, an existing bracing plate is connected to the superior flange of the cross-girder and to the inferior flange of the UPN400 cross-sections of the superior flange of the inverted Warren truss. The structural elements part of this additional bracing were modelled using both volumetric and beam elements. The respective diagonals were not found as relevant to the structural response of the investigated riveted detail, with a modelling approach with line elements being used to ensure adequate compatibility of displacements with the remaining modelled members. In the case of the cross-sectional bracing, a beam-to-solid link approach was implemented, connecting the extreme node of the beam finite element to those associated with the volumetric elements by adopting multi-point constraint equations (*master-slave*).

Regarding the boundaries of the local modelling, sections at locations without relevant stress concentrations were assumed. After the optimisation and validation procedures, it can be stated that at such cross-sections the stress and strain fields are accurately reproduced by the global model. Therefore, with a basis on the boundary nodes of the submodel, the interpolation of displacements evaluated at the nodes of the shell finite elements of the global model was adopted (shell-to-solid coupling). Assuming the well-known St. Venant's principle, it may be considered that only at these locations the distribution of stresses and strains in the submodel is disturbed, after imposing the boundary displacement conditions (*BDCOs*). Also, for the bracings, the transference of displacements was assumed from the *DOFs* of the global model to those of the submodelling, both related to beam finite elements at the same sections and nodes with similar coordinates (beam-to-beam coupling).

Concerning the existing riveted connections at the superior node with confluent diagonals located at $x=110.50$ m, except for the investigated detail, the structural elements were considered in full contact by sharing *DOFs*, which obviously does not reflect the real

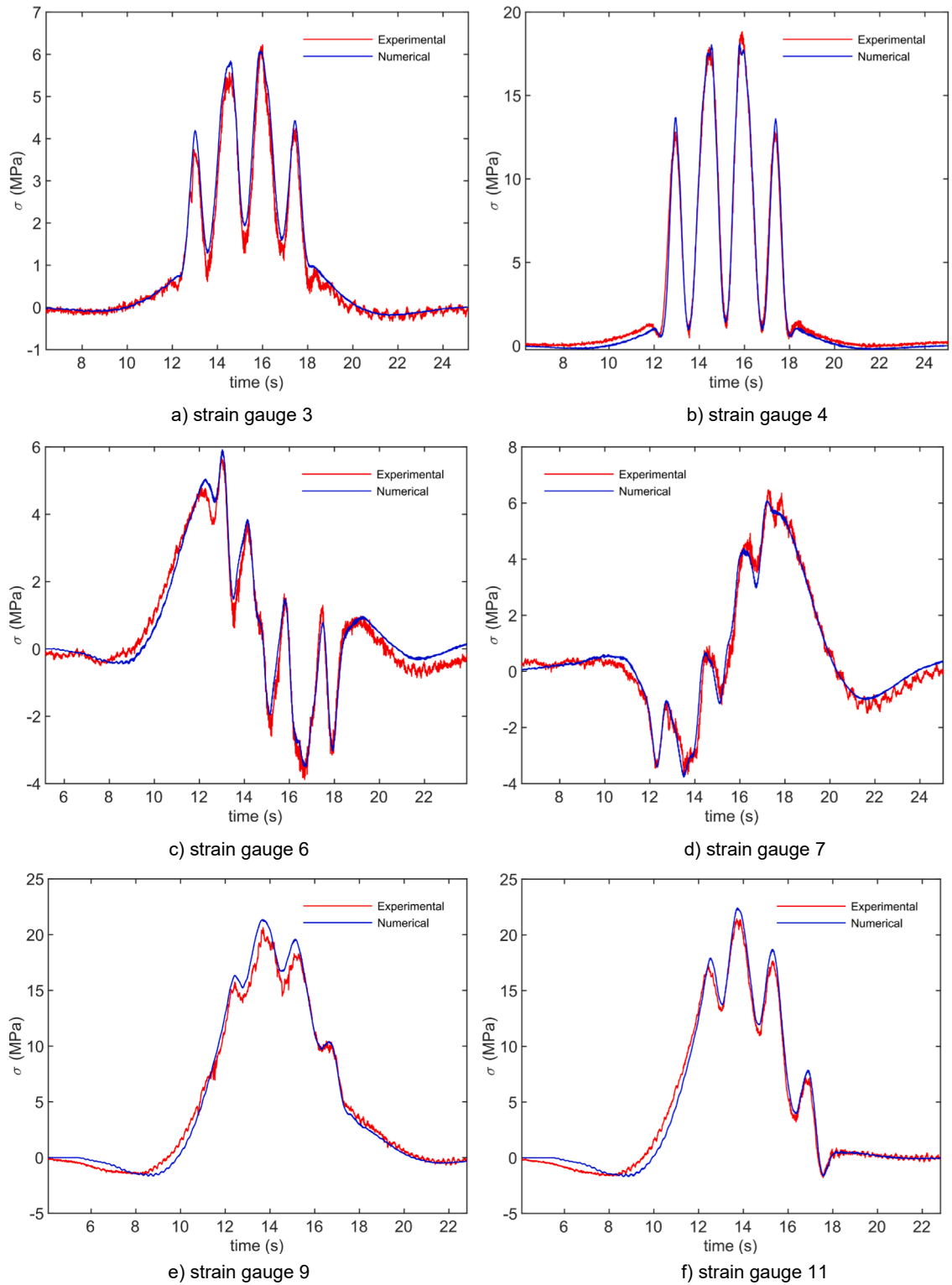


Fig. 18. Comparison between experimental and numerical stress results (shell refinement).

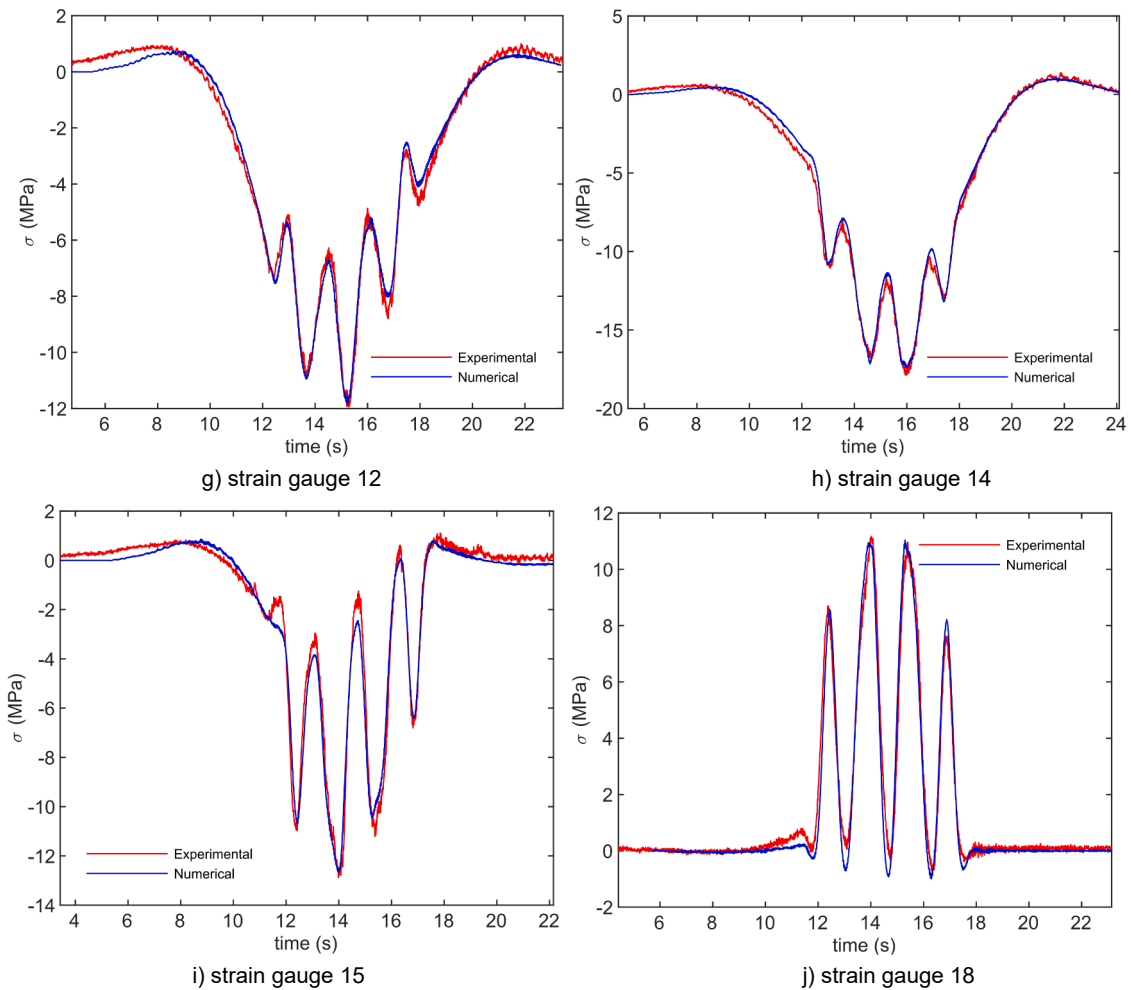


Fig. 18. (continued).

structural behaviour. However, it should be noted that the response of Civil Engineering structures is in the domain of small displacements and, for such a reason, the option assumed for the numerical modelling of these riveted details does not influence the local behaviour of the one between the diagonal and the gusset plates at $x = 109.30$ m. Furthermore, besides being irrelevant for the purpose of the present analyses, modelling all contacts and rivets would represent an excessive computational burden. On the other hand, all contacts and rivets related to the investigated riveted geometry were considered. For each side, 22 rivets with a nominal diameter of 28.05 mm (head diameter of 46 mm) were modelled according to the geometrical matrix of the rivets evaluated after the local geometrical survey (Fig. 20).

In Fig. 20, a local view of the matrix of the rivets and local views of the developed local numerical model are shown. Concerning Fig. 20 a), the local dimensions associated with the riveted length and the identification of each rivet and respective hole are presented. In this regard, it should be noted that the outlined rivets are from the inner part of the bridge (close to the track). Regarding the outer ones, a similar identification was adopted, assuming the three axes of the rivet grid dependent on the yy -coordinate as A', B' and C', i. e., the inner rivet A1 has the same xx and zz -coordinates as the outer one named A'1. Taking into account the described geometry, 20-noded volumetric elements (SOLID186 [36]) were used to conceive the submodel, except for the bracing members. For the latter, beam elements (BEAM188 [36]) were employed. Also, the contacts between the structural elements associated with the connection diagonal-to-gusset plates, located at $x=109.30$ m, were modelled using contact pair elements CONTA174-TARG170 available in ANSYS [36]. Seven surface-to-surface physical contact pairs were established: (i) rivet head - (inner or outer plate); (ii) rivet head - diagonal; (iii) rivet shank - (inner or outer plate, diagonal or gusset plate); (iv) inner plate - diagonal; (v) inner plate - outer plate; (vi) outer plate - gusset plate; and (vii) gusset plate - diagonal. For each pair, both normal and friction behaviour were admitted in order to avoid finite penetration and allow limited sliding, respectively (Coulomb model). These contact pairs were characterised considering the material properties of each steel component.

In general, linear elastic material properties were adopted according to the S355 steel grade. Nonetheless, when the crack initiation is investigated, the magnitude of local stresses may be high enough to lead to an elastoplastic stress-strain relation that may be ob-

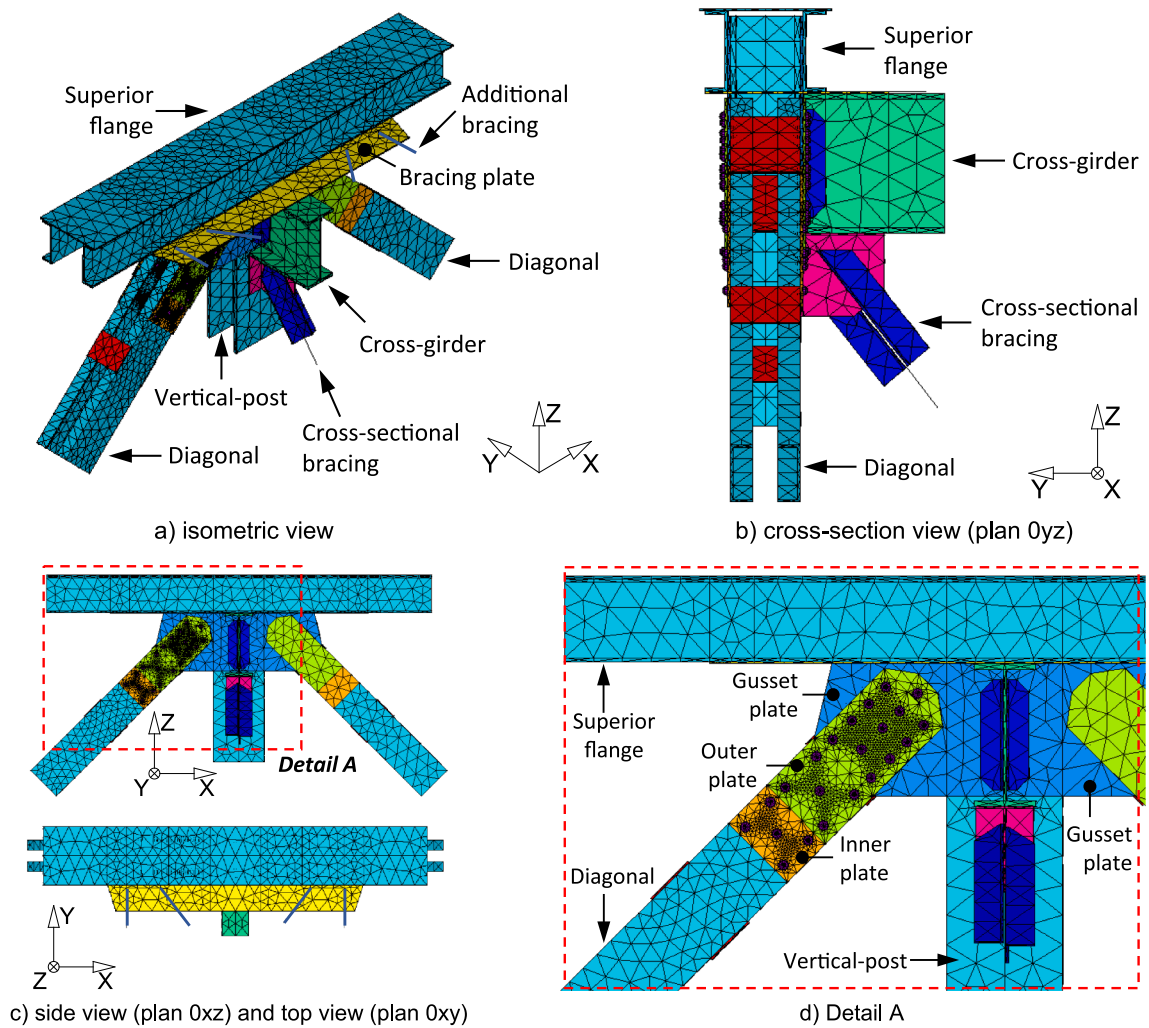


Fig. 19. Local model of the detail D.5 located at $x = 109.30$ m (local scale).

tained after analytical post-processing, as proposed by Horas *et al.* [26,27]. Thus, the necessary material parameters and the respective characteristics of the cyclic curve were assumed, i.e., $k' = 595.85$ MPa and $n' = 0.0757$ [47]. Regarding the rivets, a material defined by Young's modulus, E , of 198.7 GPa, density, ρ , equal to 7850 kg/m³, Poisson's ratio, ν , of 0.26 and friction coefficient, μ , equal to 0.15 was considered [48]. In addition, a clamping force was simulated using a negative temperature variation aiming to obtain a reduction of the length of the rivets. For such a purpose, according to the thermal expansion of the admitted material ($\alpha_y = 10^{-5} \text{ }^\circ\text{C}^{-1}$), variations of temperature were defined to install a clamping stress of 60 MPa. Due to the relevant dimension of the riveted length associated with 14 rows of staggered rivets and different heights of the shaft of the mechanical fasteners (14x2 mm or 14x3 mm, see Fig. 20 c), values between $-290 \text{ }^\circ\text{C}$ and $-390 \text{ }^\circ\text{C}$ were considered.

Once established all the geometrical and material characteristics of the nodal connection located at $x = 110.50$ m, in order to obtain a compromise between the efficiency of the calculation and the accuracy of results, a sensitivity analysis was performed to define the mesh density. As shown in Fig. 20 b), c) and d), for the structural elements associated with the investigated riveted detail, a refined mesh was adopted, aiming to obtain accurate stress and strain fields at the admissible hot-spots for the initiation of cracks. On the other hand, for those with reduced influence on the local behaviour of the riveted geometry of interest, a coarser mesh was assumed, ensuring that the response of the nodal connection is properly reproduced. 101,089 elements and 199,371 nodes were considered with a total number of *DOFs* equal to 597,411. The local detail associated with the modelling of the 44 rivets, strengthening plates and connected members (diagonal and gusset plates) led to a large numerical model. Such a fact, associated with the required nonlinear calculations, gave origin to relevant computational challenges.

After defining the numerical properties of the local submodel, preliminary analyses were performed to confirm the location of the hot-spots, which were found at the rivet holes, as expected. The modal analysis of the refined global model was carried out, allowing to evaluate the modal displacements related to the boundary conditions of the conceived submodel (*BCDO_s*), associated with 4200 vibration modes corresponding to a frequency range limited by 85.15 Hz (Fig. 21).

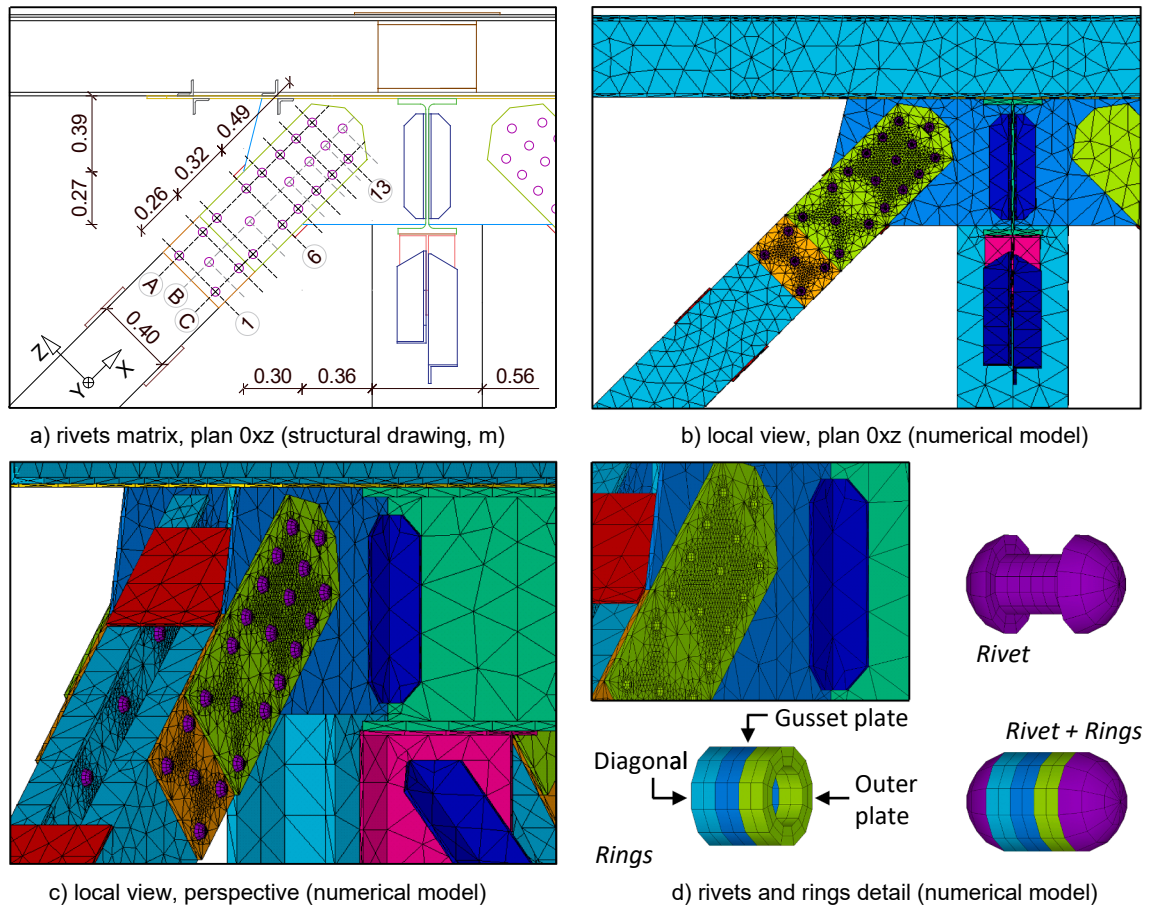


Fig. 20. Detailed view of the local model of the detail D.5 located at $x = 109.30$ m (local scale).

In Fig. 21, the locations of some of the boundaries of the submodel are shown in the global model, establishing a shell-to-solid relation. Two calculations were performed, adopting different traffic loadings: (i) the passenger train assumed to validate the refined global model, adopted at this stage to verify directly the submodelling relation considering two strain gauges of interest; and (ii) the heavy traffic mix proposed in EN1991-2 [29] to evaluate local quantities. Due to the existing contacts, the modal superposition of local parameters is not possible. As proposed by Horas et al. [27], for both loadings, the modal superposition of boundary conditions ($BDCO_s$) was performed, adopting a time step of 0.001 s that respects the maximum admissible value, $\Delta t_{max} = 1/(8f_{max})$ [49]. For each moving train, equation (7) was considered to define the amplified loading imposed on the boundaries of the submodel in the time domain, $BDCO_{s(\varphi)}(t)$.

In computational terms, the existing nonlinear contacts do not allow the modal superposition of local quantities. For each train, a set of numerical analyses should be mandatorily performed based on the conceived submodel, leading to relevant calculation times. Despite this limitation and respective reduction of the computational efficiency, such an approach makes it feasible to perform the planned analyses, which would be hardly achieved if a direct time-integration algorithm accounting for the material and contact nonlinearities was considered, due to the excessive computational burden. On the other hand, independent numerical analyses are foreseen. For each time step t , the required calculation is associated with the boundary conditions input into the submodel, which are independent of those related to the previous step $t-1$. Consequently, parallel computing algorithms may be implemented using more than one hardware setup [12]. For the riveted detail located at $x=109.30$ m, taking into account the size of the submodel, existing contact nonlinearities and reduced time step, computationally demanding numerical analyses were necessary. Therefore, a certain number of calculations were associated with two different hardware setups: (i) a personal computer (3.40GHz Intel(R) Core(TM) i7-6700CPU processor and 16GB RAM memory), used to perform 2 parallel analyses; and (ii) a workstation (2.20GHz Intel(R) Xeon(R) E5-2630CPU processor and 64GB RAM memory), in which 6 parallel calculations were held. For each train, 8 parallel analyses were carried out, dividing for each computation process the total number of steps to increase the efficiency of the calculation. In order to have a measure of the computational costs, about 4 days and 12 h of analyses were required for the normative fatigue train type 5 (longer time), while 1 day and 21 h were necessary for the normative fatigue train type 11 (shorter time).

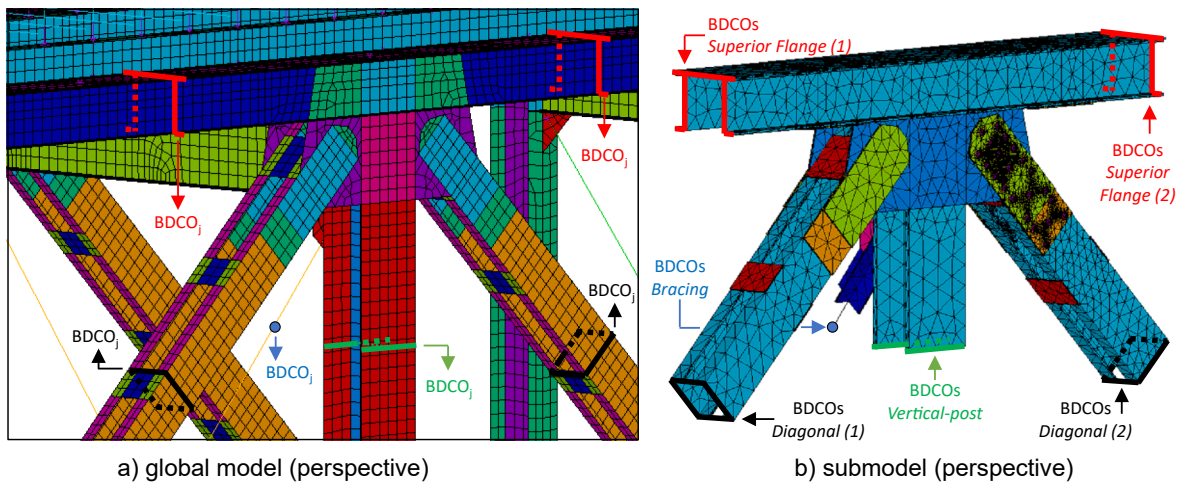


Fig. 21. Submodelling relation between the refined global model and the local model at $x = 109.30$ m (local scale).

5.2 Validation of the submodelling relation (shell-to-solid)

After fully defining the relation of the shell refinement of the global model with the conceived volumetric local model, a comparison was performed between the experimental values of interest and the numerical ones (Fig. 22).

In Fig. 22, the nominal stresses evaluated experimentally and numerically are compared for two strain gauges close to the investigated detail located at $x=109.30$ m. A good agreement was achieved, with the numerical values being obtained in the conceived submodel. Such results allowed proving the accuracy of the submodelling relation, after validating the reliability of the refined global model.

5.3 Local results

According to preliminary calculations, some multiaxiality was found at the hot-spots for the crack initiation located at the rivet holes. Nonetheless, the relevant component of the response was found to be the one related to the longitudinal axis of the diagonal, σ_{xx} (see Table 1 or Fig. 20 a)). Conservatively, aiming to evaluate the magnitudes of local stresses, the corresponding von Mises values and respective principal stress components were evaluated.

The time history for a given local stress was assessed by assuming the average of the stress fields through the thickness of the most stressed member, admitting the appearance of a thru crack. This hypothesis may be defined as a reasonable approximation to estimate the fatigue life in correspondence with the initiation of an edge crack that propagates for a certain time until reaching the full thickness. Thus, the average results obtained allowed defining the stress components properly amplified ($\sigma_{xx}, \sigma_{yy}, \sigma_{zz}, \tau_{xy}, \tau_{xz}$ and τ_{yz}), from which

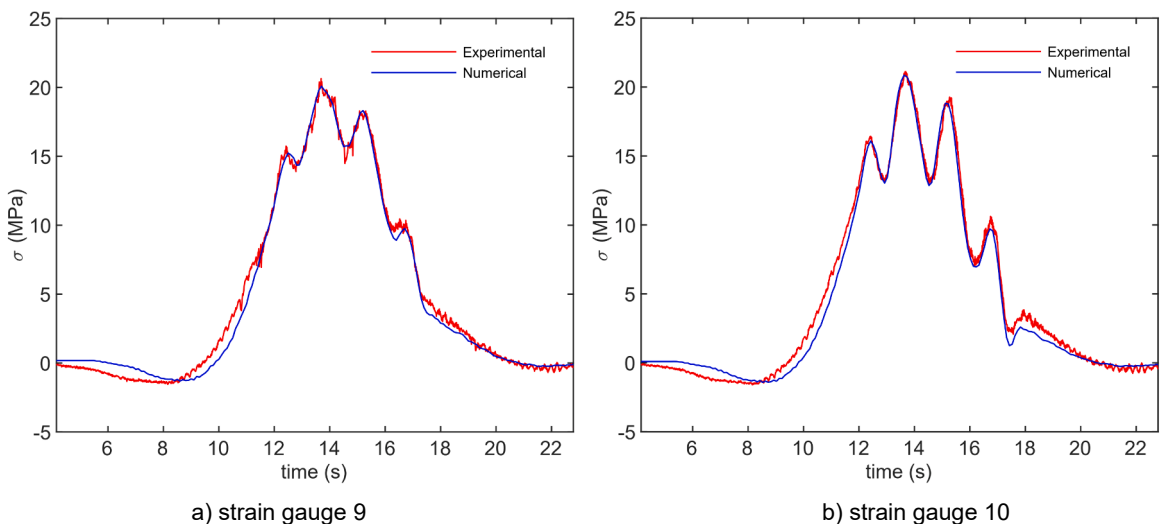


Fig. 22. Comparison between experimental and numerical stress results (submodel).

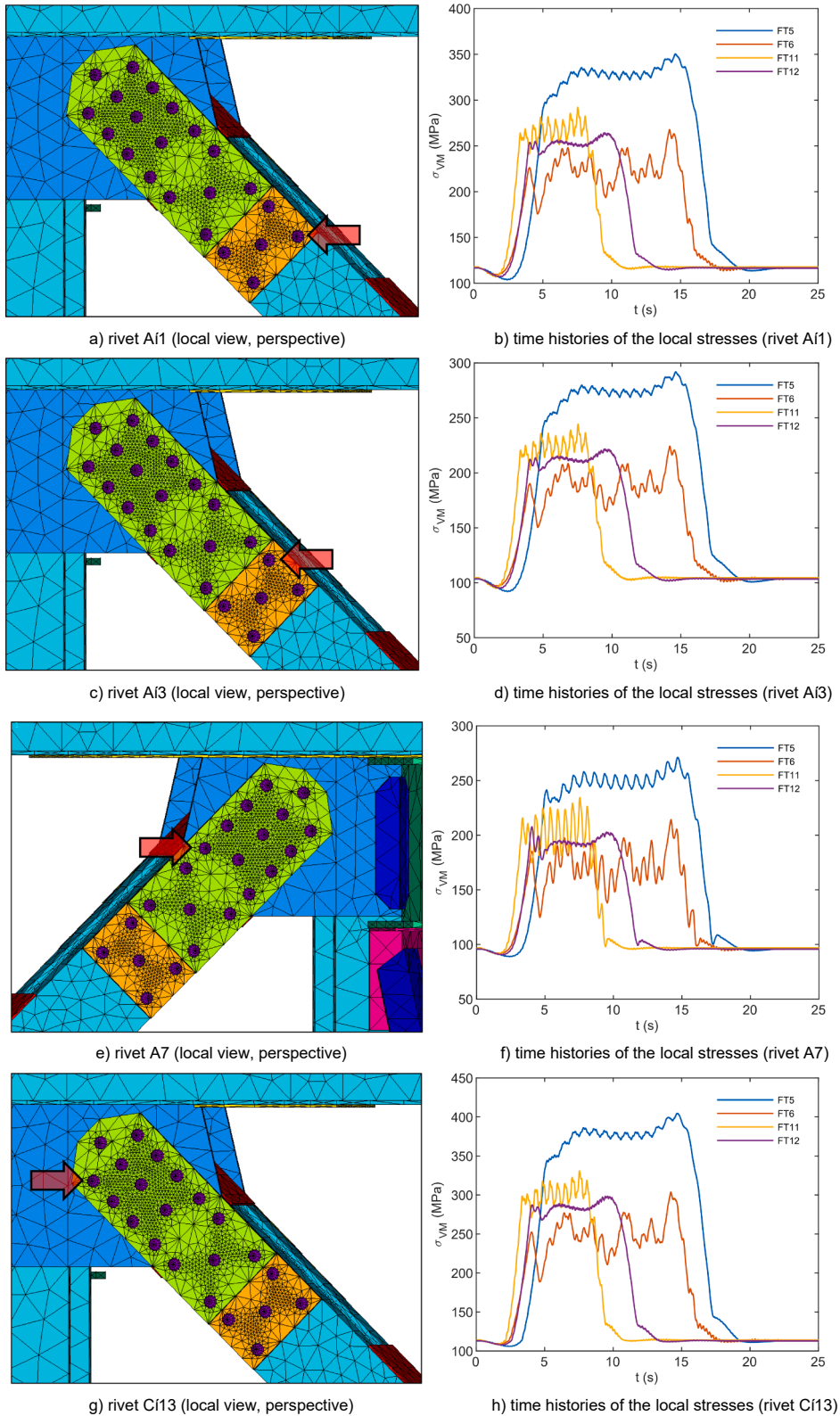


Fig. 23. Time histories of the local von Mises stresses for the considered fatigue trains.

the time histories of the principal stresses (σ_1 , σ_2 and σ_3) were calculated and the equivalent von Mises stress was computed, σ_{VM} (Fig. 23).

In Fig. 23, the local von Mises stresses at the rivet holes are shown for the trains of the considered normative heavy traffic scenario, composed of four Fatigue Trains (FT5, FT6, FT11 and FT12). The results presented were evaluated at the hot-spots located at the diagonal and the gusset plates, part of the riveted connection. Considering f_{yd} equal to 355 MPa, elastic stresses time histories were found for 40 of the 44 holes of the staggered rivets that compose the loading transference mechanism. For the hot-spots related to rivets A13, C13, A'13 and C'13, higher values than the yielding stress were computed. For the latter, a maximum value for the von Mises stress of 404.58 MPa was obtained, showing that a phenomenon of plasticity should be initiated after the first passage of the fatigue train type 5 (FT5). As proposed by Horas *et al.* [26,27], based on the computed local results, the fatigue life related to the crack initiation may be computed by implementing local methods, after performing the elastoplastic post-processing considering the Neuber or Glinka models (respectively, [20] or [21–23]). In cases of expected initiation of cracks, the remaining fatigue life associated with the propagation phase may be computed considering Linear Elastic Fracture Mechanics concepts and the defined submodelling relation, updating the cracked area for each crack increment. Such a fatigue assessment is defined as out of the scope of the present work and further calculation tasks are foreseen with a basis on the performed local stress analysis.

5.4. Main modelling recommendations

In summary, advices concerning different tasks underlying the general workflow proposed in Fig. 1 should be stressed. The characteristics of a given global model depends on the dimension of the bridge, with beam finite elements being used to model large and complex structural systems. On the other hand, for short-span bridges, a global model conceived with shell finite elements is admissible. At the global scale, i), optimisation procedures should be implemented to reduce sources of uncertainties between the numerical modelling and the real structure. After, at the member scale, ii), for fatigue-critical details, shell refinements should be incorporated into the global model, if admissible and when beam finite elements are initially assumed. These modelling improvements should allow computing nominal strain and stress measures in components related to connections with the highest damage indices. The comparison with experimental data acquired under the passage of a given train is defined as critical to verify the accuracy of the numerical results, making it possible to subsequently define multiscale relations with the solid submodels of interest, which can replicate with good reliability the real local structural response, defining boundary conditions in sections not affected by geometrical nonlinearities. Finally, at this local scale, iii), all the geometrical and material properties should be considered. In the case of riveted details, the normal and friction nonlinear contacts must be modelled, and it is advisable the modelling limited to the mechanical fasteners relevant to the loading transference mechanism investigated, due to the computational burden. A new validation of the modelling may be performed, such as that carried out at the member scale.

The progressive implementation of the multiscale modelling allows obtaining validated results compatible with different scales of analysis, with an appropriate detail at the local scale being finally reached, approximating as much as possible the numerical modelling of the real structure.

6. Conclusions

After identifying the fatigue-critical details of the Várzeas Bridge, the suggested multiscale modelling methodology was fully implemented, representing numerically and representatively, with accuracy and reliability, the structural behaviour of a given connection at all scales of interest, from the global one to the local area associated with fatigue damage. The application of the workflow proposed in Fig. 1 to such a case study led to the following main and generalisable conclusions:

- i) the challenges associated with the multiple scales of the problem are efficiently overcome;
- ii) the local results obtained at the hot-spots are in line with the real characteristics of the local behaviour of the investigated connection;
- iii) the local stress analysis gives the outcomes required for the subsequent fatigue assessment by implementing the local fatigue approaches proposed by Horas *et al.* [26,27];
- iv) the reliable numerical simulation for multiple loading scenarios is possible, in times compatible with the pace of regular Civil Engineering tasks, allowing several fatigue checks related to the initiation and propagation of cracks; and,
- v) the integrated numerical models conceived may eventually assist the future virtual replication of fatigue phenomena in real time, following a digital twinning philosophy.

Overall, the proposed efficient multiscale methodology allows investigating fatigue-critical details in line with the real structural response, providing numerical tools to be use by the bridge management authority to evaluate the structural integrity of the railway bridges of a certain network.

Declaration of Competing Interest

The authors declare that they have no known competing financial interests or personal relationships that could have appeared to influence the work reported in this paper.

Acknowledgments

This work was financially supported by: Base Funding - UIDB/04708/2020 of the CONSTRUCT - Institute of R&D In Structures and Construction - funded by national funds through the FCT/MCTES (PIDDAC) and by national funds through FCT - Fundação para a Ciência e a Tecnologia; PD/BD/114101/2015. This work was also carried out in the framework of Shift2Rail projects IN2TRACK2 [826255-H2020-S2RJU-CFM-2018] and IN2TRACK3 [101012456-H2020-S2RJU-CFM-2020].

References

- [1] European Commission, Climate Action. Transport emissions, (2019). https://ec.europa.eu/clima/policies/transport_en (accessed April 3, 2020).
- [2] C.O. Viana, H. Carvalho, J. Correia, P.A. Montenegro, R.P. Heleno, G.S. Alencar, A.M.P. de Jesus, R. Calçada, Fatigue assessment based on hot-spot stresses obtained from the global dynamic analysis and local static sub-model, *Int. J. Struct. Integr.* 12 (2019) 31–47. <https://doi.org/10.1108/IJSI-03-2019-0021>.
- [3] D. Liao, S.-P. Zhu, B. Keshtegar, G. Qian, Q. Wang, Probabilistic framework for fatigue life assessment of notched components under size effects, *Int. J. Mech. Sci.* 181 (2020) 105685, <https://doi.org/10.1016/j.ijmecsci.2020.105685>.
- [4] C.S. Horas, *Integrated Methodology for Fatigue Life Prediction of Existing Metallic Railway Bridges*, Faculty of Engineering of, the University of Porto, 2021.
- [5] C. Albuquerque, P.M.S.T. de Castro, R. Calçada, Efficient crack analysis of dynamically loaded structures using a modal superposition of stress intensity factors, *Eng. Fract. Mech.* 93 (2012) 75–91, <https://doi.org/10.1016/j.engfracmech.2012.06.009>.
- [6] D. Liao, S.-P. Zhu, G. Qian, Multiaxial fatigue analysis of notched components using combined critical plane and critical distance approach, *Int. J. Mech. Sci.* 160 (2019) 38–50, <https://doi.org/10.1016/j.ijmecsci.2019.06.027>.
- [7] CEN, Eurocode 3 - Design of steel structures, Part 1-9 Fatigue. (2010).
- [8] D. Radaj, C.M. Sonsino, W. Fricke, *Fatigue Assessment of Welded Joints by Local Approaches*, Woodhead publishing, 2006.
- [9] C. Albuquerque, A.L.L. Silva, A.M.P. de Jesus, R. Calçada, An efficient methodology for fatigue damage assessment of bridge details using modal superposition of stress intensity factors, *Int. J. Fatigue*. 81 (2015) 61–77, <https://doi.org/10.1016/j.ijfatigue.2015.07.002>.
- [10] A. Silva, *Advanced Methodologies for the Fatigue Analysis of Representative Details of Metallic Bridges*, Faculty of Engineering of, the University of Porto, 2015.
- [11] R.M. Teixeira, *Metodologias para Modelagem e Análise da Fadiga em Ligações Rebitadas com Aplicação em Pontes Metálicas Ferroviárias*, Escola Politécnica da Universidade de São Paulo (2015).
- [12] C.S. Horas, G. Alencar, A.M.P. De Jesus, R. Calçada, Development of an efficient approach for fatigue crack initiation and propagation analysis of bridge critical details using the modal superposition technique, *Eng. Fail. Anal.* 89 (2018) 118–137, <https://doi.org/10.1016/J.ENGFAILANAL.2018.03.009>.
- [13] F. Marques, J.A.F.O. Correia, A.M.P. de Jesus, Á. Cunha, E. Caetano, A.A. Fernandes, Fatigue analysis of a railway bridge based on fracture mechanics and local modelling of riveted connections, *Eng. Fail. Anal.* 94 (2018) 121–144, <https://doi.org/10.1016/j.engfailanal.2018.07.016>.
- [14] K. Kiss, L. Dunai, Stress history generation for truss bridges using multi-level models, *Comput. Struct.* 78 (1-3) (2000) 329–339.
- [15] K. Kiss, L. Dunai, Fracture mechanics based fatigue analysis of steel bridge decks by two-level cracked models, *Comput. Struct.* 80 (27-30) (2002) 2321–2331, [https://doi.org/10.1016/S0045-7949\(02\)00254-7](https://doi.org/10.1016/S0045-7949(02)00254-7).
- [16] Z.X. Li, T.Q. Zhou, T.H.T. Chan, Y. Yu, Multi-scale numerical analysis on dynamic response and local damage in long-span bridges, *Eng. Struct.* 29 (2007) 1507–1524. <https://doi.org/https://doi.org/10.1016/j.engstruct.2006.08.004>.
- [17] O.H. Basquin, The Exponential Law of Endurance Tests, *Am. Soc. Test. Mater. Proc.* 10 (1910) 625–630.
- [18] J. Morrow, Cyclic Plastic Strain Energy and Fatigue of Metals, in: *Intern. Frict. Damping, Cycl. Plast.*, ASTM International, 1965: pp. 45–87. <https://doi.org/10.1520/STP437645>.
- [19] J. Morrow, Fatigue design handbook, in: *Fatigue Prop. Met.*, No. AE-4, Society of Automotive Engineers, Warrendale, PA., 1968: pp. 21–29.
- [20] H. Neuber, Theory of stress concentration for shear-strained prismatical bodies with arbitrary nonlinear stress-strain law, *J. Appl. Mech.* 28 (1961) 544–550.
- [21] G. Glinka, Calculation of inelastic notch-tip strain-stress histories under cyclic loading, *Eng. Fract. Mech.* 22 (1985) 839–854. [https://doi.org/https://doi.org/10.1016/0013-7944\(85\)90112-2](https://doi.org/https://doi.org/10.1016/0013-7944(85)90112-2).
- [22] G. Glinka, Energy density approach to calculation of inelastic strain-stress near notches and cracks, *Eng. Fract. Mech.* 22 (1985) 485–508. [https://doi.org/https://doi.org/10.1016/0013-7944\(85\)90148-1](https://doi.org/https://doi.org/10.1016/0013-7944(85)90148-1).
- [23] G. Glinka, Relations Between the Strain Energy Density Distribution and Elastic-Plastic Stress-Strain Fields Near Cracks and Notches and Fatigue Life Calculation, *ASTM STP 942* (1988) 1022–1047, <https://doi.org/10.1520/STP245385>.
- [24] K.-J. Bathe, *Finite Element Procedures*, Prentice Hall Inc, New Jersey, 1996.
- [25] J. Chung, G.M. Hulbert, A time integration algorithm for structural dynamics with improved numerical dissipation: the generalized- α method, *J. Appl. Mech.* 60 (1993) 371–375.
- [26] C.S. Horas, J.A.F.O. Correia, A.M.P. De Jesus, P. Kripakaran, R. Calçada, Application of the modal superposition technique combined with analytical elastoplastic approaches to assess the fatigue crack initiation on structural components, *Eng. Fract. Mech.* 185 (2017) 271–283, <https://doi.org/10.1016/j.engfracmech.2017.06.001>.
- [27] C.S. Horas, A.M.P. De Jesus, R. Calçada, Efficient computational approach for fatigue assessment of riveted connections, *J. Constr. Steel Res.* 153 (2019) 1–18. <https://doi.org/https://doi.org/10.1016/j.jcsr.2018.10.005>.
- [28] R.W. Clough, J. Penzien, *Dynamics of structures*, Computers & Structures (1995).
- [29] CEN, Eurocode 1: Actions on structures, Part 2 Traffic loads Bridge. (2017).
- [30] L.R. Ticona Melo, T.N. Bittencourt, D. Ribeiro, R. Calçada, Dynamic Response of a Railway Bridge to Heavy Axle-Load Trains Considering Vehicle-Bridge Interaction, *Int. J. Struct. Stab. Dyn.* 18 (01) (2018) 1850010, <https://doi.org/10.1142/S0219455418500104>.
- [31] B. Imam, *Fatigue Analysis of Riveted Railway Bridges*, University of Surrey, 2006.
- [32] G. Kaliyaperumal, B. Imam, T. Righiniotis, Advanced dynamic finite element analysis of a skew steel railway bridge, *Eng. Struct.* 33 (2011) 181–190. <https://doi.org/https://doi.org/10.1016/j.engstruct.2010.10.003>.
- [33] F. Yan, W. Chen, Z. Lin, Prediction of fatigue life of welded details in cable-stayed orthotropic steel deck bridges, *Eng. Struct.* 127 (2016) 344–358, <https://doi.org/10.1016/j.engstruct.2016.08.055>.
- [34] H. Zhou, G. Shi, Y. Wang, H. Chen, G. De Roeck, Fatigue evaluation of a composite railway bridge based on fracture mechanics through global-local dynamic analysis, *J. Constr. Steel Res.* 122 (2016) 1–13, <https://doi.org/10.1016/j.jcsr.2016.01.014>.
- [35] I. ANSYS, ANSYS® Academic Research, Release 18.2, (2018).
- [36] I. ANSYS, ANSYS® Academic Research, Release 17, ANSYS Mechanical APDL Element Reference, Release 17 Doc. ANSYS. (2017).
- [37] A.M.P. Jesus, J.A.F.O. Correia, Fatigue Assessment of Riveted Railway Bridge Connections. Part I: Numerical Investigations, in: 7th Eur. Conf. Steel Bridg., Guimarães, Portugal, 2008.
- [38] CEN, EN10025: Hot rolled products of structural steels, (2005).
- [39] D. Ribeiro, R. Calçada, R. Delgado, M. Brehm, V. Zabel, Finite-element model calibration of a railway vehicle based on experimental modal parameters, *Veh. Syst. Dyn.* 51 (6) (2013) 821–856, <https://doi.org/10.1080/00423114.2013.778416>.
- [40] SVS, ARTEMIS Extractor Pro. 5.3 ed., (2009).
- [41] M. Brehm, V. Zabel, C. Bucher, An automatic mode pairing strategy using an enhanced modal modal assurance criterion based on modal strain energies, *J. Sound Vib.* 329 (25) (2010) 5375–5392, <https://doi.org/10.1016/j.jsv.2010.07.006>.
- [42] D. Ribeiro, R. Calçada, R. Delgado, M. Brehm, V. Zabel, Finite element model updating of a bowstring-arch railway bridge based on experimental modal parameters, *Eng. Struct.* 40 (2012) 413–435, <https://doi.org/10.1016/j.engstruct.2012.03.013>.

- [43] C. Albuquerque, *Advanced Methodologies for the Assessment of the Fatigue Behaviour of Railway Bridges*, Faculty of Engineering of, the University of Porto, 2015.
- [44] F. Marques, C. Moutinho, W.H. Hu, Á. Cunha, E. Caetano, Weigh-in-motion implementation in an old metallic railway bridge, *Eng. Struct.* 123 (2016) 15–29, <https://doi.org/10.1016/j.engstruct.2016.05.016>.
- [45] R. Pimentel, D. Ribeiro, L. Matos, A. Mosleh, R. Calçada, Bridge Weigh-in-Motion system for the identification of train loads using fiber-optic technology, *Structures.* 30 (2021) 1056–1070, <https://doi.org/10.1016/j.istruc.2021.01.070>.
- [46] B. Akesson, *Fatigue Life of Riveted Steel Bridges*, CRC Press, London, 2010 <https://doi.org/doi:10.1201/b10429-110.1201/b10429-1>.
- [47] A.M.P. de Jesus, R. Matos, B.F.C. Fontoura, C. Rebelo, L. Simões da Silva, M. Veljkovic, A comparison of the fatigue behavior between S355 and S690 steel grades, *J. Constr. Steel Res.* 79 (2012) 140–150. <https://doi.org/https://doi.org/10.1016/j.jcsr.2012.07.021>.
- [48] J.A.F.O. Correia, *An Integral Probabilistic Approach for Fatigue Lifetime Prediction of Mechanical and Structural Components*, Faculty of Engineering of, the University of Porto, 2014.
- [49] D. Ribeiro, *Comportamento Dinâmico de Pontes sob Acção de Tráfego Ferroviário de Alta Velocidade*, Faculty of Engineering of, the University of Porto, 2004.